Available online at www.sciencedirect.com
SCIENCE DIRECT®
Journal of Computational Physics 192 (2003) 36–72
JOURNAL OF COMPUTATIONAL PHYSICS
www.elsevier.com/locate/jcp

The sequential method for the black-oil reservoir simulation on unstructured grids ☆

Baoyan Li, Zhangxin Chen *, Guanren Huan

Department of Mathematics, Southern Methodist University, Box 750156, Dallas, TX 75275-0156, USA

Received 23 October 2002; received in revised form 26 June 2003; accepted 4 July 2003

Abstract

This paper presents new results for applying the sequential solution method to the black-oil reservoir simulation with unstructured grids. The fully implicit solution method has been successfully applied to reservoir simulation with unstructured grids. However, the complexity of the fully implicit method and the irregularity of the grids result in a very complicated structure of linear equation systems (LESs) and in high computational cost to solve them. To tackle this problem, the sequential method is applied to reduce the size of the LESs. To deal with instable problems caused by the low implicit degree of this method, some practical techniques are introduced to control convergence of Newton–Raphson's iterations which are exploited in the linearization of the governing equations of the black-oil model. These techniques are tested with the benchmark problem of the ninth comparative solution project (CSP) organized by the society of petroleum engineers (SPE) and applied to field-scale models of both saturated and undersaturated reservoirs. The simulation results show that the sequential method uses as little as 20.01% of the memory for solving the LESs and 23.89% of the total computational time of the fully implicit method to reach the same precision for the undersaturated reservoirs, when the same iteration control parameters are used for both solution methods. However, for the saturated reservoirs, the sequential method must use stricter iteration control parameters to reach the same precision as the fully implicit method.

Keywords: Sequential solution method; Fully implicit solution method; Control volume function approximation; Reservoir simulation; Black-oil model; Unstructured grid

1. Introduction

Fluid flow models in porous media involve large systems of nonlinear, coupled and time-dependent partial differential equations. An important problem in reservoir simulation is to develop stable, efficient,

☆ This research is supported in part by National Science Foundation grants DMS-9972147 and INT-9901498.
* Corresponding author.
E-mail addresses: bli@mail.smu.edu (B. Li), zchen@post.cis.smu.edu, zchen@mail.smu.edu (Z. Chen), huan@golem.math.smu.edu (G. Huan).

0021-9991/$ - see front matter © 2003 Elsevier B.V. All rights reserved.
doi:10.1016/S0021-9991(03)00346-2

robust, and accurate solution methods for solving these coupled equations. Essentially, there are three types of solution methods in reservoir simulation: the IMPES (implicit in pressure and explicit in saturation), the fully implicit, and the sequential.

The IMPES solution method [19] works well for reservoir simulation of two-phase incompressible flow. Recently, we have developed an improved IMPES method [5], which is capable of solving two-phase coning problems. However, the IMPES method is not efficient and robust for fluid flows having strong nonlinearities, such as the black-oil and compositional flows. To improve the efficiency of the IMPES method, adaptive IMPES methods were developed [18,24], which use a switching criterion, based on the Courant–Friedrichs–Lewy (CFL) condition, to determine when grid blocks should be treated implicitly and when they should be treated explicitly. An IMPES stability criterion for the multidimensional black oil and compositional models was discussed in [7] as well.

The fully implicit solution method, which is also called the simultaneous solution method [8], solves all of the coupled nonlinear equations simultaneously. This method is stable and can take very large time steps, while its stability is maintained. However, this method requires lots of memory and has high computational cost, compared with the IMPES and sequential methods. It will become very challenging for huge simulation models.

The sequential solution method [16] splits the coupled system of nonlinear governing equations of reservoir simulation up into individual equations and solves each of these equations separately and implicitly. It greatly reduces the size of the resulting LESs and results in low memory and computational cost to solve these LESs. This method is less stable but more efficient than the fully implicit method, and more stable but less efficient than the IMPES method. It has been recently applied to the numerical solution of complex flow problems such as the black-oil and compositional models [4,6,20,21]. However, in these papers, numerical results have been obtained for one-dimensional model problems.

To model accurately and efficiently irregularly geometrical and geological features and flow patterns of a reservoir, gridding techniques of unstructured girds and various discretization methods have been developed in the past 10 years [1]. Heinrich [11] introduced the perpendicular bisector (PEBI) method. Forsyth [9] developed control volume finite element (CVFE) grids and the CVFE method for thermal reservoir simulation. Fung et al. [10] applied them to commercial thermal reservoir simulators. Verma and Aziz [22] improved the CVFE method to deal with permeability tensors using three-dimensional CVFE grids. Li et al. [12,14] recently introduced the control volume function approximation (CVFA) method into the black-oil reservoir simulation using arbitrarily shaped grids and checked the stability and accuracy of this method to deal with the ''bubble point'' and coning problems [15]. For reservoir simulation using the black-oil model on unstructured grids, only the fully implicit solution method has been used for solving the governing equations of this model. Because the connection between grid blocks is irregular for unstructured grids, the Jacobian matrices for these grids are much more complicated than those for structured grids. Furthermore, the full implicity and grid irregularity require a great amount of memory and high computational cost to solve the LESs. Particularly, for field-scale reservoir simulation, this becomes a very serious problem.

In this paper, we attack the above problem from a different angle. We apply the sequential solution method to the black-oil reservoir simulation with unstructured grids to reduce memory and computational cost. As noted, because of the low implicit degree, this method may introduce instability in solution. Some rules are introduced to select time steps and to perform time step cutting for a modeling process. In particular, practical termination conditions are adopted in the Newton–Raphson iteration procedure which is used for solving nonlinear equations. Also, a special technique is used for dealing with the bubble point problem. To deal with arbitrarily shaped unstructured grids, we apply the CVFA method to discretize the governing equations of the black oil model, since this method can directly discretize these equations on arbitrarily shaped control volumes and can guarantee that the flux is continuous across an interface between two neighboring control volumes. We test this approach with both the ninth SPE CSP benchmark

problem and field-scale simulation models by comparing the simulation results from it with those from the fully implicit method.

The rest of this paper is organized as follows. Section 2 presents the black-oil model, its linearization by the Newton–Raphson procedure, and its discretization by the CVFA method. The sequential solution method is described in Section 3. The practical techniques to handle stability and convergence are introduced in Section 4. Numerical experiments are presented in Section 5. Conclusions are given in Section 6. Finally, the linearization and discretization of the black-oil model and the derivation of pressure equations are described in Appendixes A, B, and C, respectively.

2. The black-oil model and its discretization

The black-oil model is a simplified compositional model. For this model, it is assumed that the hydrocarbon components can be divided into methane and a heavy oil component in a stock tank at the standard pressure. It is also assumed that no mass transfer occurs between the water phase and the other two phases (oil and gas) and no volatile oil exits.

Let ϕ and K denote the porosity and permeability of a porous medium $\Omega \subset \Re^3$, s_α, μ_α, p_α, $\mathbf{u}_\alpha$, B_α, and $K_{r\alpha}$ be the saturation, viscosity, pressure, volumetric velocity, formation volume factor, and relative permeability of the α phase, $\alpha = \mathrm{w}, \mathrm{o}, \mathrm{g}$, respectively, and R_{so} be the gas solubility. Then the mass conservation equations of the black-oil model are [2]

$$-\nabla \cdot \left(\frac{\rho_{\mathrm{WS}}}{B_{\mathrm{w}}} \mathbf{u}_{\mathbf{w}} \right) + q_{\mathrm{w}} = \frac{\partial}{\partial t} \left(\phi \frac{\rho_{\mathrm{WS}}}{B_{\mathrm{w}}} s_{\mathrm{w}} \right) \tag{2.1}$$

for the water component,

$$-\nabla \cdot \left(\frac{\rho_{\mathrm{OS}}}{B_{\mathrm{o}}} \mathbf{u}_{\mathbf{o}} \right) + q_{\mathrm{o}} = \frac{\partial}{\partial t} \left(\phi \frac{\rho_{\mathrm{OS}}}{B_{\mathrm{o}}} s_{\mathrm{o}} \right) \tag{2.2}$$

for the oil component,

$$-\nabla \cdot \left(\frac{\rho_{\mathrm{GS}}}{B_{\mathrm{g}}} \mathbf{u}_{\mathbf{g}} + \frac{R_{\mathrm{so}} \rho_{\mathrm{GS}}}{B_{\mathrm{o}}} \mathbf{u}_{\mathbf{o}} \right) + q_{\mathrm{g}} = \frac{\partial}{\partial t} \left[\phi \left(\frac{\rho_{\mathrm{GS}}}{B_{\mathrm{g}}} s_{\mathrm{g}} + \frac{R_{\mathrm{so}} \rho_{\mathrm{GS}}}{B_{\mathrm{o}}} s_{\mathrm{o}} \right) \right] \tag{2.3}$$

for the gas component, where $\rho_{\beta S}$ is the density of the β component at standard conditions (stock tank), $\beta = \mathrm{W}, \mathrm{O}, \mathrm{G}$, q_α is the mass flow rate of the α phase at wells, and

$$q_{\mathrm{g}} = q_{\mathrm{g}}^{\mathrm{G}} + q_{\mathrm{o}}^{\mathrm{G}}.$$

The volumetric velocity of the α phase is represented by Darcy's law

$$\mathbf{u}_\alpha = -\frac{K K_{r\alpha}}{\mu_\alpha} \nabla \Phi_\alpha, \quad \alpha = \mathrm{g}, \mathrm{o}, \mathrm{w}, \tag{2.4}$$

where the potential Φ_α of the α phase is given by

$$\Phi_\alpha = p_\alpha - \rho_\alpha \tilde{\boldsymbol{g}} D, \quad \alpha = \mathrm{w}, \mathrm{o}, \mathrm{g}, \tag{2.5}$$

ρ_α represents the density of the α phase, $\tilde{\boldsymbol{g}}$ is the gravitational constant, and D is the depth function. The saturations of the water, oil, and gas phases satisfy the constraint

$$s_{\mathrm{w}} + s_{\mathrm{o}} + s_{\mathrm{g}} = 1. \tag{2.6}$$

Furthermore, the phase pressures are related by the capillary pressures p_{cow} and p_{cgo}:

$$p_{\mathrm{cow}} = p_{\mathrm{o}} - p_{\mathrm{w}}, \quad p_{\mathrm{cgo}} = p_{\mathrm{g}} - p_{\mathrm{o}}. \tag{2.7}$$

Finally, the mass flow rates of wells are given by Peaceman's formulas [17]

$$\begin{aligned}
q_{\mathrm{o}} &= \sum_{k=1}^{N_{\mathrm{w}}} \sum_{m=1}^{M_{\mathrm{w}k}} \frac{2\pi\Delta z_{k,m}}{\ln(r_{e,k,m}/r_{c,k}) + s_{k,m}} \frac{KK_{\mathrm{ro}}\rho_{\mathrm{OS}}}{\mu_{\mathrm{o}}B_{\mathrm{o}}} \left[p_{\mathrm{bh},k} - p_{\mathrm{o}} - \rho_{\mathrm{o}}\tilde{g}(D_{\mathrm{w},k} - D)\right]\delta_{k,m},\\
q_{\mathrm{w}} &= \sum_{k=1}^{N_{\mathrm{w}}} \sum_{m=1}^{M_{\mathrm{w}k}} \frac{2\pi\Delta z_{k,m}}{\ln(r_{e,k,m}/r_{c,k}) + s_{k,m}} \frac{KK_{\mathrm{rw}}\rho_{\mathrm{WS}}}{\mu_{\mathrm{w}}B_{\mathrm{w}}} \left[p_{\mathrm{bh},k} - p_{\mathrm{w}} - \rho_{\mathrm{w}}\tilde{g}(D_{\mathrm{w},k} - D)\right]\delta_{k,m},\\
q_{\mathrm{g}}^{\mathrm{G}} &= \sum_{k=1}^{N_{\mathrm{w}}} \sum_{m=1}^{M_{\mathrm{w}k}} \frac{2\pi\Delta z_{k,m}}{\ln(r_{e,k,m}/r_{c,k}) + s_{k,m}} \frac{KK_{\mathrm{rg}}\rho_{\mathrm{GS}}}{\mu_{\mathrm{g}}B_{\mathrm{g}}} \left[p_{\mathrm{bh},k} - p_{\mathrm{g}} - \rho_{\mathrm{g}}\tilde{g}(D_{\mathrm{w},k} - D)\right]\delta_{k,m},\\
q_{\mathrm{o}}^{\mathrm{G}} &= \sum_{k=1}^{N_{\mathrm{w}}} \sum_{m=1}^{M_{\mathrm{w}k}} \frac{2\pi\Delta z_{k,m}}{\ln(r_{e,k,m}/r_{c,k}) + s_{k,m}} \frac{KK_{\mathrm{ro}}R_{\mathrm{so}}\rho_{\mathrm{GS}}}{\mu_{\mathrm{o}}B_{\mathrm{o}}} \left[p_{\mathrm{bh},k} - p_{\mathrm{o}} - \rho_{\mathrm{o}}\tilde{g}(D_{\mathrm{w},k} - D)\right]\delta_{k,m},
\end{aligned} \tag{2.8}$$

where $\delta_{k,m} = \delta(\mathbf{x} - \mathbf{x}_{k,m})$ (the Dirac delta function at $\mathbf{x}_{k,m}$), N_{w} is the total number of wells, $M_{\mathrm{w},k}$ is the total number of perforated zones of the kth well, $s_{k,m}$, $\Delta z_{k,m}$, and $\mathbf{x}_{k,m}$ are the skin factor, segment length, and central location of the mth perforated zone of the kth well, $r_{c,k}$ denotes the wellbore radius of the kth well, $r_{e,k,m}$ is the drainage radius of the kth well at the grid block in which $\mathbf{x}_{k,m}$ is located, respectively, and $p_{\mathrm{bh},k}$ is the bottom hole pressure of the kth well at datum $D_{\mathrm{w},k}$.

The model is completed by specifying boundary and initial conditions. In this paper we consider no flow boundary conditions

$$\mathbf{u}_{\alpha} \cdot \mathbf{n} = 0, \quad \alpha = \mathrm{w}, \mathrm{o}, \mathrm{g}, \quad \mathbf{x} \in \partial\Omega, \tag{2.9}$$

where $\mathbf{n}$ is the outward unit norm to the boundary $\partial\Omega$ of the reservoir domain Ω. The initial conditions depend on the state of a reservoir. When all gas dissolves into the oil phase, there is no gas phase present, i.e., $s_{\mathrm{g}} = 0$. In such a case, the reservoir is said to be in the undersaturated state. If all three phases co-exist, the reservoir is referred to as in the saturated state. In the undersaturated state, we use $p = p_{\mathrm{o}}$, s_{w}, and p_{b} as the unknowns, where p_{b} is the bubble point pressure; see Appendix A. The corresponding initial conditions are

$$\begin{aligned}
&p(\mathbf{x}, 0) = p^0(\mathbf{x}), \quad \mathbf{x} \in \Omega,\\
&p_{\mathrm{b}}(\mathbf{x}, 0) = p_{\mathrm{b}}^0(\mathbf{x}), \quad \mathbf{x} \in \Omega,\\
&s_{\mathrm{w}}(\mathbf{x}, 0) = s_{\mathrm{w}}^0(\mathbf{x}), \quad \mathbf{x} \in \Omega.
\end{aligned} \tag{2.10}$$

In the saturated state, we employ $p = p_{\mathrm{o}}$, s_{w}, and s_{o} as the unknowns. In this case, the initial conditions become

$$\begin{aligned}
&p(\mathbf{x}, 0) = p^0(\mathbf{x}), \quad \mathbf{x} \in \Omega,\\
&s_{\mathrm{w}}(\mathbf{x}, 0) = s_{\mathrm{w}}^0(\mathbf{x}), \quad \mathbf{x} \in \Omega,\\
&s_{\mathrm{o}}(\mathbf{x}, 0) = s_{\mathrm{o}}^0(\mathbf{x}), \quad \mathbf{x} \in \Omega.
\end{aligned} \tag{2.11}$$

Various well constraints need to be taken into account. For an injection well, two kinds of well constraints are permitted. They are, respectively, the constant bottom hole pressure and constant injection flow rate. In the former case, the bottom hole pressure is fixed:

$$p_{\mathrm{bh},k} = P_{\mathrm{bh},k}, \tag{2.12}$$

where k is the sequential number of the well which has this kind of well control and $P_{\mathrm{bh},k}$ is the given bottom hole pressure of this well. In the latter case, the injection flow rate controls for water and gas injection wells are, respectively,

$$\begin{aligned}
&\sum_{m=1}^{M_{\mathrm{w},k}} \int_{V_{k,m}} \mathrm{WI}_{k,m} \frac{K_{\mathrm{rwmax}}\rho_{\mathrm{WS}}}{\mu_{\mathrm{w}}B_{\mathrm{w}}} \Big[p_{\mathrm{bh}} - p_{\mathrm{w}} - \rho_{\mathrm{w}}\tilde{\boldsymbol{g}}(D_{\mathrm{w},k} - D)\Big]\delta_{k,m}\,\mathrm{d}\mathbf{x} = Q_{\mathrm{W},k},\\
&\sum_{m=1}^{M_{\mathrm{w},k}} \int_{V_{k,m}} \mathrm{WI}_{k,m} \frac{K_{\mathrm{rgmax}}\rho_{\mathrm{GS}}}{\mu_{\mathrm{g}}B_{\mathrm{g}}} \Big[p_{\mathrm{bh}} - p_{\mathrm{g}} - \rho_{\mathrm{g}}\tilde{\boldsymbol{g}}(D_{\mathrm{w},k} - D)\Big]\delta_{k,m}\,\mathrm{d}\mathbf{x} = Q^{\mathrm{G}}_{\mathrm{g},k},
\end{aligned} \tag{2.13}$$

where $Q_{\mathrm{W},k}$ and $Q^{\mathrm{G}}_{\mathrm{g},k}$ are the given water and gas injection rates for the water and gas injection rate controls, respectively, $K_{\mathrm{r}\alpha\,\mathrm{max}}$ is the maximum relative permeability of the α phase, $\alpha = \mathrm{w}, \mathrm{g}$, $V_{k,m}$ denotes the control volume in which the mth perforated zone of the kth well falls, and the well index $\mathrm{WI}_{k,m}$ is defined as

$$\mathrm{WI}_{k,m} = \frac{2\pi\Delta z_{k,m}K}{\ln(r_{e,k,m}/r_{c,k}) + s_{k,m}}.$$

For a production well, there are three constraints: a constant bottom hole pressure, a constant total flow rate, and a constant total liquid production rate. The constant bottom hole pressure takes the same form as (2.12). For an oil production well, the oil production rate control is

$$\sum_{m=1}^{M_{\mathrm{w},k}} \int_{V_{k,m}} \mathrm{WI}_{k,m} \frac{K_{\mathrm{ro}}\rho_{\mathrm{OS}}}{\mu_{\mathrm{o}}B_{\mathrm{o}}} \Big[p_{\mathrm{bh}} - p_{\mathrm{o}} - \rho_{\mathrm{o}}\tilde{\boldsymbol{g}}(D_{\mathrm{w},k} - D)\Big]\delta_{k,m}\,\mathrm{d}\mathbf{x} = Q_{\mathrm{O},k}, \tag{2.14}$$

where $Q_{\mathrm{O},k}$ is the given oil production rate. For a gas production well, the production rate control is

$$\begin{aligned}
&\sum_{m=1}^{M_{\mathrm{w},k}} \int_{V_{k,m}} \mathrm{WI}_{k,m} \frac{K_{\mathrm{rg}}\rho_{\mathrm{GS}}}{\mu_{\mathrm{g}}B_{\mathrm{g}}} \Big[p_{\mathrm{bh}} - p_{\mathrm{g}} - \rho_{\mathrm{g}}\tilde{\boldsymbol{g}}(D_{\mathrm{w},k} - D)\Big]\delta_{k,m}\,\mathrm{d}\mathbf{x}\\
&\quad + \sum_{m=1}^{M_{\mathrm{w},k}} \int_{V_{k,m}} \mathrm{WI}_{k,m} \frac{K_{\mathrm{ro}}R_{\mathrm{so}}\rho_{\mathrm{GS}}}{\mu_{\mathrm{o}}B_{\mathrm{o}}} \Big[p_{\mathrm{bh}} - p_{\mathrm{o}} - \rho_{\mathrm{o}}\tilde{\boldsymbol{g}}(D_{\mathrm{w},k} - D)\Big]\delta_{k,m}\,\mathrm{d}\mathbf{x} = Q^{\mathrm{G}}_{k},
\end{aligned} \tag{2.15}$$

where Q^{G}_{k} is the given gas production rate of the kth well. Note that the gas–oil ratio (GOR) at a perforated zone of a well must be less than a certain limit; over this limit, that perforated zone needs to be shut down. The liquid flow rate control is only applicable for an oil production well and is of the form

$$\begin{aligned}
&\sum_{m=1}^{M_{\mathrm{w},k}} \int_{V_{k,m}} \mathrm{WI}_{k,m} \frac{K_{\mathrm{rw}}\rho_{\mathrm{WS}}}{\mu_{\mathrm{w}}B_{\mathrm{w}}} \Big[p_{\mathrm{bh}} - p_{\mathrm{w}} - \rho_{\mathrm{w}}\tilde{\boldsymbol{g}}(D_{\mathrm{w},k} - D)\Big]\delta_{k,m}\,\mathrm{d}\mathbf{x}\\
&\quad + \sum_{m=1}^{M_{\mathrm{w}k}} \int_{V_{k,m}} \mathrm{WI}_{k,m} \frac{K_{\mathrm{ro}}\rho_{\mathrm{OS}}}{\mu_{\mathrm{o}}B_{\mathrm{o}}} \Big[p_{\mathrm{bh}} - p_{\mathrm{o}} - \rho_{\mathrm{o}}\tilde{\boldsymbol{g}}(D_{\mathrm{w},k} - D)\Big]\delta_{k,m}\,\mathrm{d}\mathbf{x} = Q_{\mathrm{L},k},
\end{aligned} \tag{2.16}$$

where $Q_{\mathrm{L},k}$ is the given total liquid production rate of the kth well. Also, the water cut, which is defined as the ratio of the water production rate to the sum of the water and oil production rates, at a perforated zone of a well with this kind of well constraint must be less than a certain limit; otherwise, that perforated zone needs to be shut down.

We use both the sequential and fully implicit methods to solve the above nonlinear equations and apply the CVFA method to discretize them in space. To model accurately the geometrical and geological features of a reservoir, a hybrid grid needs to be used for reservoir simulation. Since the CVFA method can directly

discretize an equation on an arbitrarily shaped grid and is especially suitable for the hybrid grid reservoir simulation, we apply this method to dealing with the discretization of the governing equations of the black-oil model and the treatment of wells.

We very briefly review the discretization of the black-oil model using the CVFA and the linearization of this model using Newton–Raphson's procedure. For more details, refer to Appendixes A and B. Since the unknowns on control volumes can be different under different states of a reservoir, the integral forms of the governing equations on each control volume are solved, respectively, under the undersaturated and saturated states. In the undersaturated state, the lth iteration values of the water and oil potentials on boundary e_{ij} of a control volume V_i at the $(n+1)$th time step are approximated by

$$\begin{aligned}(\Phi_{\mathrm{wh}})_l^{(n+1)} &= \sum_{r=0}^{R_{ij}} (\Phi^i_{\mathrm{w}_{j,r}})_l^{(n+1)} \phi^i_{j,r}(\mathbf{x}), \quad \mathbf{x} \in e_{ij},\\ (\Phi_{\mathrm{oh}})_l^{(n+1)} &= \sum_{r=0}^{R_{ij}} (\Phi^i_{\mathrm{o}_{j,r}})_l^{(n+1)} \phi^i_{j,r}(\mathbf{x}), \quad \mathbf{x} \in e_{ij},\end{aligned} \tag{2.17}$$

where l refers to the iteration number of Newton–Raphson's iterations, $\phi^i_{j,r}(\mathbf{x})$, $r = 0, 1, \ldots, R_{i,j}$, are the shape functions, $R_{ij}+1$ is the total number of interpolation points for $(\Phi_{\alpha h})_l^{(n+1)}$ on e_{ij}, and $(\Phi^i_{\alpha_{j,r}})_l^{(n+1)}$ denotes the nodal value of $(\Phi_{\alpha h})_l^{(n+1)}$, $\alpha = \mathrm{w}, \mathrm{o}$. Since δp, δp_{b}, and δs_{w} at grid points in all time steps need to be obtained for this state, we approximate the lth iteration values of these variables at the $(n+1)$th time step by

$$\begin{aligned}(\delta p_{\mathrm{h}})_l^{(n+1)} &= \sum_{r=0}^{R_{ij}} (\delta p^i_{j,r})_l^{(n+1)} \phi^i_{j,r}(\mathbf{x}), \quad \mathbf{x} \in e_{ij},\\ (\delta s_{\mathrm{wh}})_l^{(n+1)} &= \sum_{r=0}^{R_{ij}} (\delta s^i_{\mathrm{w}_{j,r}})_l^{(n+1)} \phi^i_{j,r}(\mathbf{x}), \quad \mathbf{x} \in e_{ij},\\ (\delta p_{\mathrm{b_h}})_l^{(n+1)} &= \sum_{r=0}^{R_{ij}} (\delta p^i_{\mathrm{b}_{j,r}})_l^{(n+1)} \phi^i_{j,r}(\mathbf{x}), \quad \mathbf{x} \in e_{ij}.\end{aligned} \tag{2.18}$$

We substitute these interpolants into the linearized governing equations given in Appendix A.1 to obtain the discrete equations, which are given in Appendix B. In these discrete equations, the lth iteration values of increments $(\delta p^i_{j,r})_l^{(n+1)}$, $(\delta s^i_{\mathrm{w}_{j,r}})_l^{(n+1)}$, and $(\delta p^i_{\mathrm{b}_{j,r}})_l^{(n+1)}$ at the $(n+1)$th time step at nodes $\mathbf{x}^i_{j,r}$ are the unknowns to be solved for. For a well with a flow rate control, the increment of its bottom hole pressure also needs to be obtained. After these increments are obtained, the iteration solutions at grid point $\mathbf{x}_i$ and the bottom hole pressure of the kth well are updated by

$$\begin{aligned}(p_i)_{l+1}^{(n+1)} &= (p_i)_l^{(n+1)} + (\delta p_i)_l^{(n+1)},\\ (s_{\mathrm{w}_i})_{l+1}^{(n+1)} &= (s_{\mathrm{w}_i})_l^{(n+1)} + (\delta s_{\mathrm{w}_i})_l^{(n+1)},\\ (p_{\mathrm{b}_i})_{l+1}^{(n+1)} &= (p_{\mathrm{b}_i})_l^{(n+1)} + (\delta p_{\mathrm{b}_i})_l^{(n+1)},\\ (p_{\mathrm{bh},k})_{l+1}^{(n+1)} &= (p_{\mathrm{bh},k})_l^{(n+1)} + (\delta p_{\mathrm{bh},k})_l^{(n+1)}.\end{aligned} \tag{2.19}$$

Similarly, in the saturated state, we approximate the lth iteration values of the water, oil, and gas potentials at the $(n+1)$th time step by

$$
\begin{aligned}
(\Phi_{\mathrm{wh}})_l^{(n+1)} &= \sum_{r=0}^{R_{ij}} (\Phi^i_{\mathrm{w}_{j,r}})_l^{(n+1)} \phi^i_{j,r}(\mathbf{x}), \quad \mathbf{x} \in e_{ij}, \\
(\Phi_{\mathrm{oh}})_l^{(n+1)} &= \sum_{r=0}^{R_{ij}} (\Phi^i_{\mathrm{o}_{j,r}})_l^{(n+1)} \phi^i_{j,r}(\mathbf{x}), \quad \mathbf{x} \in e_{ij}, \\
(\Phi_{gh})_l^{(n+1)} &= \sum_{r=0}^{R_{ij}} (\Phi^i_{g_{j,r}})_l^{(n+1)} \phi^i_{j,r}(\mathbf{x}), \quad \mathbf{x} \in e_{ij},
\end{aligned}
\tag{2.20}
$$

and approximate the unknowns $(\delta p)_l^{(n+1)}$, $(\delta s_{\mathrm{w}})_l^{(n+1)}$, and $(\delta s_{\mathrm{o}})_l^{(n+1)}$ by

$$
\begin{aligned}
(\delta p_{\mathrm{h}})_l^{(n+1)} &= \sum_{r=0}^{R_{ij}} (\delta p^i_{j,r})_l^{(n+1)} \phi^i_{j,r}(\mathbf{x}), \quad \mathbf{x} \in e_{ij}, \\
(\delta s_{\mathrm{wh}})_l^{(n+1)} &= \sum_{r=0}^{R_{ij}} (\delta s^i_{\mathrm{w}_{j,r}})_l^{(n+1)} \phi^i_{j,r}(\mathbf{x}), \quad \mathbf{x} \in e_{ij}, \\
(\delta s_{\mathrm{oh}})_l^{(n+1)} &= \sum_{r=0}^{R_{ij}} (\delta s^i_{\mathrm{o}_{j,r}})_l^{(n+1)} \phi^i_{j,r}(\mathbf{x}), \quad \mathbf{x} \in e_{ij}.
\end{aligned}
\tag{2.21}
$$

We substitute them into the linearized governing equations in Appendix A.2 to get the discrete equations, which are listed in Appendix B. The iteration solution values at grid point $\mathbf{x}_i$ and the kth well, which has a flow rate control, are updated by

$$
\begin{aligned}
(p_i)_{l+1}^{(n+1)} &= (p_i)_l^{(n+1)} + (\delta p_i)_l^{(n+1)}, \\
(s_{\mathrm{w}_i})_{l+1}^{(n+1)} &= (s_{\mathrm{w}_i})_l^{(n+1)} + (\delta s_{\mathrm{w}_i})_l^{(n+1)}, \\
(s_{\mathrm{o}_i})_{l+1}^{(n+1)} &= (s_{\mathrm{o}_i})_l^{(n+1)} + (\delta s_{\mathrm{o}_i})_l^{(n+1)}, \\
(p_{\mathrm{bh},k})_{l+1}^{(n+1)} &= (p_{\mathrm{bh},k})_l^{(n+1)} + (\delta p_{\mathrm{bh},k})_l^{(n+1)}.
\end{aligned}
\tag{2.22}
$$

We end with a remark that different states at different places in a reservoir can occur; i.e., the saturated and undersaturated states can co-exist. In this case, the governing equations on each control volume are linearized and discretized according to the state in this volume.

3. Sequential solution method

The idea of the sequential solution method is to decouple the governing equations into the pressure, water saturation, and gas saturation equation in the saturated state (or into the pressure, water saturation, and bubble point pressure equations in the undersaturated state) and to solve them separately and implicitly in different states. This can be accomplished with the linearized and discretized equations given in Appendix B.

3.1. Pressure equations

The pressure equation can be obtained from the governing equations and well control equations given in Appendix B. For a given grid block i, $(\delta s^i_{\mathrm{w}_{j,r}})_l^{(n+1)}$, $(\delta s^i_{\mathrm{o}_{j,r}})_l^{(n+1)}$ (for the saturated state) or $(\delta p^i_{\mathrm{b}_{j,r}})_l^{(n+1)}$ (for the undersaturated state) are set to zero on the left-hand sides of these equations, and these unknowns are eliminated on the right-hand sides of these equations in an appropriate way to obtain the pressure equation; see Appendix C for more details.

The well controls are implicitly treated; i.e., we linearize the control equations of wells. If the kth well has the control of the bottom hole pressure, from (2.12) we set

$$\delta p_{\mathrm{bh},k} = 0. \tag{3.1}$$

For injection wells, we linearize the well control equations in (2.13) into

$$\begin{aligned}\sum_{m=1}^{M_{\mathrm{w},k}} \int_{V_{k,m}} \Bigg\{ & \mathrm{WI}_{k,m} \left(\frac{K_{\mathrm{rwmax}} \rho_{\mathrm{WS}}}{\mu_{\mathrm{w}} B_{\mathrm{w}}} \right)_l^{(n+1)} \left[(\delta p_{\mathrm{bh},k})_l^{(n+1)} - (\delta p)_l^{(n+1)} \right] \\ & + (q_{\mathrm{w},k,m})_l^{(n+1)} \left[1 + \frac{\mu_{\mathrm{w}} B_{\mathrm{w}}}{\rho_{\mathrm{WS}}} \frac{\partial}{\partial p} \left(\frac{\rho_{\mathrm{WS}}}{\mu_{\mathrm{w}} B_{\mathrm{w}}} \right) \delta p \right]_l^{(n+1)} \Bigg\} \delta_{k,m} \, \mathrm{d}\mathbf{x} = Q_{\mathrm{W},k}, \end{aligned} \tag{3.2}$$

for the water injection rate control of the kth well, and

$$\begin{aligned}\sum_{m=1}^{M_{\mathrm{w},k}} \int_{V_{k,m}} \Bigg\{ & \mathrm{WI}_{k,m} \left(\frac{K_{\mathrm{rgmax}} \rho_{\mathrm{GS}}}{\mu_{\mathrm{g}} B_{\mathrm{g}}} \right)_l^{(n+1)} \left[(\delta p_{\mathrm{bh},k})_l^{(n+1)} - (\delta p)_l^{(n+1)} \right] \\ & + (q_{\mathrm{g},k,m})_l^{(n+1)} \left[1 + \frac{\mu_{\mathrm{g}} B_{\mathrm{g}}}{\rho_{\mathrm{GS}}} \frac{\partial}{\partial p} \left(\frac{\rho_{\mathrm{GS}}}{\mu_{\mathrm{g}} B_{\mathrm{g}}} \right) \delta p \right]_l^{(n+1)} \Bigg\} \delta_{k,m} \, \mathrm{d}\mathbf{x} = Q_{\mathrm{g},k}^{\mathrm{G}}, \end{aligned} \tag{3.3}$$

for the gas injection rate control of the kth well, where $q_{\mathrm{w},k,m}$ and $q_{\mathrm{g},k,m}$ are calculated by

$$\begin{aligned} q_{\mathrm{w},k,m} &= \mathrm{WI}_{k,m} \frac{K_{\mathrm{rwmax}} \rho_{\mathrm{WS}}}{\mu_{\mathrm{w}} B_{\mathrm{w}}} \Big[p_{\mathrm{bh}} - p_{\mathrm{w}} - \rho_{\mathrm{w}} \tilde{\boldsymbol{g}} (D_{\mathrm{w},k} - D) \Big], \\ q_{\mathrm{g},k,m} &= \mathrm{WI}_{k,m} \frac{K_{\mathrm{rgmax}} \rho_{\mathrm{GS}}}{\mu_{\mathrm{w}} B_{\mathrm{w}}} \Big[p_{\mathrm{bh}} - p_{\mathrm{g}} - \rho_{\mathrm{g}} \tilde{\boldsymbol{g}} (D_{\mathrm{w},k} - D) \Big]. \end{aligned}$$

Also, for the gas, oil, and liquid production rate control, the well control equations are, respectively, linearized into

$$\begin{aligned}\sum_{m=1}^{M_{\mathrm{w},k}} \int_{V_{k,m}} \Bigg\{ & \mathrm{WI}_{k,m} \frac{K_{\mathrm{rg}} \rho_{\mathrm{GS}}}{\mu_{\mathrm{g}} B_{\mathrm{g}}} (\delta p_{\mathrm{bh},k} - \delta p) + q_{\mathrm{g},k,m}^{\mathrm{G}} \left[1 + \frac{\mu_{\mathrm{g}} B_{\mathrm{g}}}{\rho_{\mathrm{GS}}} \frac{\partial}{\partial p} \left(\frac{\rho_{\mathrm{GS}}}{\mu_{\mathrm{g}} B_{\mathrm{g}}} \right) \delta p \right] \\ & + \mathrm{WI}_{k,m} \frac{K_{\mathrm{ro}} R_{\mathrm{so}} \rho_{\mathrm{GS}}}{\mu_{\mathrm{o}} B_{\mathrm{o}}} (\delta p_{\mathrm{bh},k} - \delta p) \\ & + q_{\mathrm{o},k,m}^{\mathrm{G}} \left[1 + \frac{\mu_{\mathrm{o}} B_{\mathrm{o}}}{R_{\mathrm{so}} \rho_{\mathrm{GS}}} \frac{\partial}{\partial p} \left(\frac{R_{\mathrm{so}} \rho_{\mathrm{GS}}}{\mu_{\mathrm{o}} B_{\mathrm{o}}} \right) \delta p \right] \Bigg\}_l^{(n+1)} \delta_{k,m} \, \mathrm{d}\mathbf{x} = Q_k^{\mathrm{G}}, \\ \sum_{m=1}^{M_{\mathrm{w},k}} \int_{V_{k,m}} \Bigg\{ & \mathrm{WI}_{k,m} \frac{K_{\mathrm{ro}} \rho_{\mathrm{OS}}}{\mu_{\mathrm{o}} B_{\mathrm{o}}} (\delta p_{\mathrm{bh},k} - \delta p) \\ & + q_{\mathrm{o},k,m} \left[1 + \frac{\mu_{\mathrm{o}} B_{\mathrm{o}}}{\rho_{\mathrm{OS}}} \frac{\partial}{\partial p} \left(\frac{\rho_{\mathrm{OS}}}{\mu_{\mathrm{o}} B_{\mathrm{o}}} \right) \delta p \right] \Bigg\}_l^{(n+1)} \delta_{k,m} \, \mathrm{d}\mathbf{x} = Q_{\mathrm{O},k}, \\ \sum_{m=1}^{M_{\mathrm{w},k}} \int_{V_{k,m}} \Bigg\{ & \mathrm{WI}_{k,m} \frac{K_{\mathrm{rw}} \rho_{\mathrm{WS}}}{\mu_{\mathrm{w}} B_{\mathrm{w}}} (\delta p_{\mathrm{bh},k} - \delta p) \\ & + q_{\mathrm{w},k,m} \left[1 + \frac{\mu_{\mathrm{w}} B_{\mathrm{w}}}{\rho_{\mathrm{WS}}} \frac{\partial}{\partial p} \left(\frac{\rho_{\mathrm{WS}}}{\mu_{\mathrm{w}} B_{\mathrm{w}}} \right) \delta p \right] + \mathrm{WI}_{k,m} \frac{K_{\mathrm{ro}} \rho_{\mathrm{OS}}}{\mu_{\mathrm{o}} B_{\mathrm{o}}} (\delta p_{\mathrm{bh},k} - \delta p) \\ & + q_{\mathrm{o},k,m} \left[1 + \frac{\mu_{\mathrm{o}} B_{\mathrm{o}}}{\rho_{\mathrm{OS}}} \frac{\partial}{\partial p} \left(\frac{\rho_{\mathrm{OS}}}{\mu_{\mathrm{o}} B_{\mathrm{o}}} \right) \delta p \right] \Bigg\}_l^{(n+1)} \delta_{k,m} \, \mathrm{d}\mathbf{x} = Q_{\mathrm{L},k}, \end{aligned} \tag{3.4}$$

where $q^{\mathrm{G}}_{\mathrm{o},k,m}$ and $q_{\mathrm{o},k,m}$ are calculated by

$$q^{\mathrm{G}}_{\mathrm{o},k,m} = \mathrm{WI}_{k,m}\frac{K_{\mathrm{ro}}R_{\mathrm{so}}\rho_{\mathrm{GS}}}{\mu_{\mathrm{o}}B_{\mathrm{o}}}\Big[p_{\mathrm{bh}} - p_{\mathrm{o}} - \rho_{\mathrm{o}}\tilde{g}(D_{\mathrm{w},k} - D)\Big],$$
$$q_{\mathrm{o},k,m} = \mathrm{WI}_{k,m}\frac{K_{\mathrm{ro}}\rho_{\mathrm{OS}}}{\mu_{\mathrm{o}}B_{\mathrm{o}}}\Big[p_{\mathrm{bh}} - p_{\mathrm{o}} - \rho_{\mathrm{o}}\tilde{g}(D_{\mathrm{w},k} - D)\Big].$$

The pressure equations given in Appendix C and the well control Eqs. (3.2)–(3.4) are solved simultaneously to get the pressure increments at grid points and the bottom hole pressure increments of wells.

3.2. Water saturation equation

If we substitute the pressure increments obtained from the pressure equations into the governing equation of the water component given in Appendix B, we can get the water saturation equation

$$\begin{aligned}
&\sum_{j=1}^{N_i}\sum_{r=0}^{R_{ij}}\int_{e_{ij}}\left\{\left[\frac{K\rho_{\mathrm{WS}}}{\mu_{\mathrm{w}}B_{\mathrm{w}}}\frac{\partial K_{\mathrm{rw}}}{\partial s_{\mathrm{w}}}\right]_l^{(n+1)}(\delta s_{\mathrm{w}})_l^{(n+1)}\right\}(\Phi^i_{\mathrm{w}_{j,r}})_l^{(n+1)}\nabla\phi^i_{j,r}(\mathbf{x})\cdot\mathbf{n}\,\mathrm{d}A\\
&\quad-\sum_{j=1}^{N_i}\sum_{r=0}^{R_{ij}}\int_{e_{ij}}\left[\frac{KK_{\mathrm{rw}}}{\mu_{\mathrm{w}}}\frac{\rho_{\mathrm{WS}}}{B_{\mathrm{w}}}\left(\frac{\partial p_{\mathrm{cow}}}{\partial s_{\mathrm{w}}}\delta s_{\mathrm{w}}\right)^i_{j,r}\nabla\phi^i_{j,r}(\mathbf{x})\right]_l^{(n+1)}\cdot\mathbf{n}\,\mathrm{d}A\\
&\quad+\sum_{k=1}^{N_{\mathrm{w}}}\sum_{m=1}^{M_{\mathrm{w},k}}\int_{V_i}\left\{\frac{q_{\mathrm{w},k,m}}{K_{\mathrm{rw}}}\frac{\partial K_{\mathrm{rw}}}{\partial s_{\mathrm{w}}}\delta s_{\mathrm{w}}\right\}_l^{(n+1)}\delta_{k,m}\,\mathrm{d}\mathbf{x}-\frac{V_i}{\Delta t_n}\left\{\left(\phi\frac{\rho_{\mathrm{WS}}}{B_{\mathrm{w}}}\right)_i(\delta s_{\mathrm{w}})_i\right\}_l^{(n+1)}=Q_{\mathrm{w},i},
\end{aligned}\tag{3.5}$$

for control volume V_i, $i = 1, 2, \ldots, N$, where

$$\begin{aligned}
Q_{\mathrm{w},i} = &-\sum_{j=1}^{N_i}\sum_{r=0}^{R_{ij}}\int_{e_{ij}}\left\{\frac{KK_{\mathrm{rw}}}{\mu_{\mathrm{w}}}\frac{\rho_{\mathrm{WS}}}{B_{\mathrm{w}}}+KK_{\mathrm{rw}}\frac{\partial}{\partial p}\left(\frac{\rho_{\mathrm{WS}}}{\mu_{\mathrm{w}}B_{\mathrm{w}}}\right)\delta p\right\}_l^{(n+1)}(\Phi^i_{\mathrm{w}_{j,r}})_l^{(n+1)}\times\nabla\phi^i_{j,r}(\mathbf{x})\cdot\mathbf{n}\,\mathrm{d}A\\
&-\sum_{j=1}^{N_i}\sum_{r=0}^{R_{ij}}\int_{e_{ij}}\left[\frac{KK_{\mathrm{rw}}}{\mu_{\mathrm{w}}}\frac{\rho_{\mathrm{WS}}}{B_{\mathrm{w}}}\delta p^i_{j,r}\right]_l^{(n+1)}\nabla\phi^i_{j,r}(\mathbf{x})\cdot\mathbf{n}\,\mathrm{d}A\\
&-\sum_{k=1}^{N_{\mathrm{w}}}\sum_{m=1}^{M_{\mathrm{w},k}}\int_{V_i}\left\{(q_{\mathrm{w},k,m})_l^{(n+1)}-\left[\mathrm{WI}_{k,m}\frac{K_{\mathrm{rw}}\rho_{\mathrm{WS}}}{\mu_{\mathrm{w}}B_{\mathrm{w}}}\delta p\right]_l^{(n+1)}\right.\\
&\left.+\left[\frac{\mu_{\mathrm{w}}B_{\mathrm{w}}}{\rho_{\mathrm{WS}}}q_{\mathrm{w},k,m}\frac{\partial}{\partial p}\left(\frac{\rho_{\mathrm{WS}}}{\mu_{\mathrm{w}}B_{\mathrm{w}}}\right)\delta p\right]_l^{(n+1)}+\mathrm{WI}_{k,m}\left(\frac{K_{\mathrm{rw}}\rho_{\mathrm{WS}}}{\mu_{\mathrm{w}}B_{\mathrm{w}}}\right)_l^{(n+1)}(\delta p_{\mathrm{bh},k})_l^{(n+1)}\right\}\delta_{k,m}\,\mathrm{d}\mathbf{x}\\
&+\frac{V_i}{\Delta t_n}\left\{\left(\phi\frac{\rho_{\mathrm{WS}}}{B_{\mathrm{w}}}s_{\mathrm{w}}\right)_l^{(n+1)}-\left(\phi\frac{\rho_{\mathrm{WS}}}{B_{\mathrm{w}}}s_{\mathrm{w}}\right)^{(n)}+\left[c_r\phi_a\frac{\rho_{\mathrm{WS}}}{B_{\mathrm{w}}}s_{\mathrm{w}}+\phi s_{\mathrm{w}}\frac{\partial}{\partial p}\left(\frac{\rho_{\mathrm{WS}}}{B_{\mathrm{w}}}\right)\right]_l^{(n+1)}(\delta p)_l^{(n+1)}\right\}_{\mathbf{x}=\mathbf{x}_i},
\end{aligned}$$

where $\mathbf{x}_i$ is the centroid of V_i and c_r and ϕ_a are the compressibility and porosity of rock, respectively. We solve Eq. (3.5) to obtain the water saturation increment $(\delta s_{\mathrm{w}})_l^{(n+1)}$ at grid points.

3.3. Oil saturation and bubble point pressure equations

Since the third unknown at any grid point is different under the different state of a reservoir, the oil saturation equation and bubble point pressure equation are derived under the saturated and undersaturated states, respectively.

For the saturated state, if the oil phase exists, the knowns $(\delta p)_l^{(n+1)}$, $(\delta p_{\mathrm{bh}})_l^{(n+1)}$, and $(\delta s_{\mathrm{w}})_l^{(n+1)}$ at grid points are substituted into the governing equation of the oil component given in Appendix B to obtain the oil saturation equation

$$
\begin{aligned}
&-\sum_{j=1}^{N_i}\sum_{r=0}^{R_{ij}}\int_{e_{ij}}\left(\frac{K\rho_{\mathrm{OS}}}{\mu_{\mathrm{o}}B_{\mathrm{o}}}\frac{\partial K_{\mathrm{ro}}}{\partial s_{\mathrm{g}}}\delta s_{\mathrm{o}}\right)_l^{(n+1)}(\Phi^i_{\mathrm{o}_{j,r}})_l^{(n+1)}\nabla\phi^i_{j,r}(\mathbf{x})\cdot\mathbf{n}\,\mathrm{d}A\\
&\quad-\sum_{k=1}^{N_{\mathrm{w}}}\sum_{m=1}^{M_{\mathrm{w},k}}\int_{V_i}\left(\frac{q_{\mathrm{o},k,m}}{K_{\mathrm{ro}}}\frac{\partial K_{\mathrm{ro}}}{\partial s_{\mathrm{g}}}\delta s_{\mathrm{o}}\right)_l^{(n+1)}\delta_{k,m}\,\mathrm{d}\mathbf{x}-\frac{V_i}{\Delta t_n}\left\{\left(\phi\frac{\rho_{\mathrm{OS}}}{B_{\mathrm{o}}}\delta s_{\mathrm{o}}\right)_i\right\}_l^{(n+1)}=Q_{\mathrm{O},i},
\end{aligned}
\tag{3.6}
$$

for control volume V_i, $i=1,2,\ldots,N$, where

$$
\begin{aligned}
Q_{\mathrm{O},i}=&-\sum_{j=1}^{N_i}\sum_{r=0}^{R_{ij}}\int_{e_{ij}}\left\{\left(\frac{KK_{\mathrm{ro}}}{\mu_{\mathrm{o}}}\frac{\rho_{\mathrm{OS}}}{B_{\mathrm{o}}}\right)_l^{(n+1)}+\left[KK_{\mathrm{ro}}\frac{\partial}{\partial p}\left(\frac{\rho_{\mathrm{OS}}}{\mu_{\mathrm{o}}B_{\mathrm{o}}}\right)\right]_l^{(n+1)}(\delta p)_l^{(n+1)}\right.\\
&\left.+\left[\frac{K\rho_{\mathrm{OS}}}{\mu_{\mathrm{o}}B_{\mathrm{o}}}\left(\frac{\partial K_{\mathrm{ro}}}{\partial s_{\mathrm{w}}}-\frac{\partial K_{\mathrm{ro}}}{\partial s_{\mathrm{g}}}\right)\delta s_{\mathrm{w}}\right]_l^{(n+1)}\right\}(\Phi^i_{\mathrm{o}_{j,r}})_l^{(n+1)}\nabla\phi^i_{j,r}(\mathbf{x})\cdot\mathbf{n}\,\mathrm{d}A\\
&-\sum_{j=1}^{N_i}\sum_{r=0}^{R_{ij}}\int_{e_{ij}}\left[\frac{KK_{\mathrm{ro}}}{\mu_{\mathrm{o}}}\frac{\rho_{\mathrm{OS}}}{B_{\mathrm{o}}}(\delta p^i_{j,r})\right]_l^{(n+1)}\nabla\phi^i_{j,r}(\mathbf{x})\cdot\mathbf{n}\,\mathrm{d}A\\
&-\sum_{k=1}^{N_{\mathrm{w}}}\sum_{m=1}^{M_{\mathrm{w},k}}\int_{V_i}\left\{(q_{\mathrm{o},k,m})_l^{(n+1)}-\left[\mathrm{WI}_{k,m}\frac{K_{\mathrm{ro}}\rho_{\mathrm{OS}}}{\mu_{\mathrm{o}}B_{\mathrm{o}}}\delta p\right]_l^{(n+1)}+\left[\frac{\mu_{\mathrm{o}}B_{\mathrm{o}}}{\rho_{\mathrm{OS}}}q_{\mathrm{o},k,m}\frac{\partial}{\partial p}\left(\frac{\rho_{\mathrm{OS}}}{\mu_{\mathrm{o}}B_{\mathrm{o}}}\right)\delta p\right]_l^{(n+1)}\right.\\
&\left.+\left[\frac{q_{\mathrm{o},k,m}}{K_{\mathrm{ro}}}\left(\frac{\partial K_{\mathrm{ro}}}{\partial s_{\mathrm{w}}}-\frac{\partial K_{\mathrm{ro}}}{\partial s_{\mathrm{g}}}\right)\right]_l^{(n+1)}(\delta s_{\mathrm{w}})_l^{(n+1)}+\mathrm{WI}_{k,m}\left(\frac{K_{\mathrm{ro}}\rho_{\mathrm{OS}}}{\mu_{\mathrm{o}}B_{\mathrm{o}}}\right)_l^{(n+1)}(\delta p_{\mathrm{bh},k})_l^{(n+1)}\right\}\delta_{k,m}\,\mathrm{d}\mathbf{x}\\
&+\frac{V_i}{\Delta t_n}\left\{\left(\phi\frac{\rho_{\mathrm{OS}}}{B_{\mathrm{o}}}s_{\mathrm{o}}\right)_l^{(n+1)}-\left(\phi\frac{\rho_{\mathrm{OS}}}{B_{\mathrm{o}}}s_{\mathrm{o}}\right)^{(n)}+\left[c_r\phi_a\frac{\rho_{\mathrm{OS}}}{B_{\mathrm{o}}}s_{\mathrm{o}}+\phi s_{\mathrm{o}}\frac{\partial}{\partial p}\left(\frac{\rho_{\mathrm{OS}}}{B_{\mathrm{o}}}\right)\right]_l^{(n+1)}(\delta p)_l^{(n+1)}\right\}_{\mathbf{x}=\mathbf{x}_i}.
\end{aligned}
$$

For the undersaturated state, the knowns $(\delta p)_l^{(n+1)}$, $(\delta p_{\mathrm{bh},k})_l^{(n+1)}$, and $(\delta s_{\mathrm{w}})_l^{(n+1)}$ at grid points are substituted into the governing equation of the gas component given in Appendix B to obtain the bubble point pressure equation

$$
\begin{aligned}
&\sum_{j=1}^{N_i}\sum_{r=0}^{R_{ij}}\int_{e_{ij}}\left\{\left[KK_{\mathrm{ro}}\frac{\partial}{\partial p_{\mathrm{b}}}\left(\frac{R_{\mathrm{so}}\rho_{\mathrm{GS}}}{\mu_{\mathrm{o}}B_{\mathrm{o}}}\right)\right]_l^{(n+1)}(\delta p_{\mathrm{b}})_l^{(n+1)}\right\}(\Phi^i_{\mathrm{o}_{j,r}})_l^{(n+1)}\nabla\phi^i_{j,r}(\mathbf{x})\cdot\mathbf{n}\,\mathrm{d}A\\
&\quad+\sum_{k=1}^{N_{\mathrm{w}}}\sum_{m=1}^{M_{\mathrm{w},k}}\int_{V_i}\left\{\left(\frac{\mu_{\mathrm{o}}B_{\mathrm{o}}}{R_{\mathrm{so}}\rho_{\mathrm{GS}}}q^{\mathrm{G}}_{\mathrm{o},k,m}\right)_l^{(n+1)}\left[\frac{\partial}{\partial p_{\mathrm{b}}}\left(\frac{R_{\mathrm{so}}\rho_{\mathrm{GS}}}{\mu_{\mathrm{o}}B_{\mathrm{o}}}\right)\right]_l^{(n+1)}(\delta p_{\mathrm{b}})_l^{(n+1)}\right\}\delta_{k,m}\,\mathrm{d}\mathbf{x}\\
&\quad-\frac{V_i}{\Delta t_n}\left\{\left[\phi s_{\mathrm{o}}\frac{\partial}{\partial p_{\mathrm{b}}}\left(\frac{R_{\mathrm{so}}\rho_{\mathrm{GS}}}{B_{\mathrm{o}}}\right)\right]_l^{(n+1)}(\delta p_{\mathrm{b}})_l^{(n+1)}\right\}_{\mathbf{x}=\mathbf{x}_i}=Q_{\mathrm{G},i},
\end{aligned}
\tag{3.7}
$$

where

$$
\begin{aligned}
Q_{\mathrm{G},i} = & -\sum_{j=1}^{N_i}\sum_{r=0}^{R_{ij}}\int_{e_{ij}}\left\{\left(\frac{KK_{\mathrm{ro}}}{\mu_{\mathrm{o}}}\frac{R_{\mathrm{so}}\rho_{\mathrm{GS}}}{B_{\mathrm{o}}}\right)_l^{(n+1)} + \left[KK_{\mathrm{ro}}\frac{\partial}{\partial p}\left(\frac{R_{\mathrm{so}}\rho_{\mathrm{GS}}}{\mu_{\mathrm{o}}B_{\mathrm{o}}}\right)\right]_l^{(n+1)}(\delta p)_l^{(n+1)}\right\} \\
& \times (\Phi^i_{\mathrm{o}_{j,r}})_l^{(n+1)}\nabla\phi^i_{j,r}(\mathbf{x})\cdot\mathbf{n}\,\mathrm{d}A - \sum_{j=1}^{N_i}\sum_{r=0}^{R_{ij}}\int_{e_{ij}}\left[\frac{KK_{\mathrm{ro}}}{\mu_{\mathrm{o}}}\frac{R_{\mathrm{so}}\rho_{\mathrm{GS}}}{B_{\mathrm{o}}}(\delta p^i_{j,r})\nabla\phi^i_{j,r}(\mathbf{x})\right]_l^{(n+1)}\cdot\mathbf{n}\,\mathrm{d}A \\
& -\sum_{k=1}^{N_{\mathrm{w}}}\sum_{m=1}^{M_{\mathrm{w},k}}\int_{V_i}\left\{(q^{\mathrm{G}}_{\mathrm{o},k,m})_l^{(n+1)} - \left[\mathrm{WI}_{k,m}\frac{K_{\mathrm{ro}}R_{\mathrm{so}}\rho_{\mathrm{GS}}}{\mu_{\mathrm{o}}B_{\mathrm{o}}}\delta p\right]_l^{(n+1)} + \left[\frac{\mu_{\mathrm{o}}B_{\mathrm{o}}}{R_{\mathrm{so}}\rho_{\mathrm{GS}}}q^{\mathrm{G}}_{\mathrm{o},k,m}\frac{\partial}{\partial p}\left(\frac{R_{\mathrm{so}}\rho_{\mathrm{GS}}}{\mu_{\mathrm{o}}B_{\mathrm{o}}}\right)\delta p\right]_l^{(n+1)}\right. \\
& \left. + \left(\frac{q^{\mathrm{G}}_{\mathrm{o},k,m}}{K_{\mathrm{ro}}}\frac{\partial K_{\mathrm{ro}}}{\partial s_{\mathrm{w}}}\right)_l^{(n+1)}(\delta s_{\mathrm{w}})_l^{(n+1)} + \mathrm{WI}_{k,m}\left(\frac{K_{\mathrm{ro}}R_{\mathrm{so}}\rho_{\mathrm{GS}}}{\mu_{\mathrm{o}}B_{\mathrm{o}}}\right)_l^{(n+1)}(\delta p_{\mathrm{bh},k})_l^{(n+1)}\right\}\delta_{k,m}\,\mathrm{d}\mathbf{x} \\
& + \frac{V_i}{\Delta t_n}\left\{\left(\phi\frac{R_{\mathrm{so}}\rho_{\mathrm{GS}}}{B_{\mathrm{o}}}s_{\mathrm{o}}\right)_l^{(n+1)} - \left(\phi\frac{R_{\mathrm{so}}\rho_{\mathrm{GS}}}{B_{\mathrm{o}}}s_{\mathrm{o}}\right)^{(n)} - \left(\phi\frac{R_{\mathrm{so}}\rho_{\mathrm{GS}}}{B_{\mathrm{o}}}\right)_l^{(n+1)}(\delta s_{\mathrm{w}})_l^{(n+1)}\right. \\
& \left. + \left[c_r\phi_a\frac{R_{\mathrm{so}}\rho_{\mathrm{GS}}}{B_{\mathrm{o}}}s_{\mathrm{o}} + \phi s_{\mathrm{o}}\frac{\partial}{\partial p}\left(\frac{R_{\mathrm{so}}\rho_{\mathrm{GS}}}{B_{\mathrm{o}}}\right)\right]_l^{(n+1)}(\delta p)_l^{(n+1)}\right\}_{\mathbf{x}=\mathbf{x}_i}.
\end{aligned}
$$

4. Convergence control

As noted, compared with the fully implicit solution method, the sequential solution method has lower implicity. It may introduce instability into Newton–Raphson's iterations. Hence some practical techniques are needed for selecting time steps and controlling convergence of the Newton–Raphson iterations.

4.1. Treatment of the "bubble point" problem

It is very important to deal properly with the bubble point problem for controlling convergence of Newton–Raphson's iterations. The state of a reservoir can change from saturated to undersaturated or vice versa. To determine a proper state during the state transition is the bubble point problem. If the bubble point problem can promptly be recognized and reasonable unknowns can be selected for different states of a reservoir in a Newton–Raphson iteration, it will benefit for determining a proper convergent direction and speed up convergence.

To treat properly the bubble point problem, we figure out the triggers which cause the transition of states of a reservoir using the state machine [3], shown in Fig. 1. We can see that a point in the reservoir can stay in either the saturated state or the undersaturated state. Furthermore, from the lth iteration to the $(l+1)$th iteration in a Newton–Raphson iteration process at the $(n+1)$th time step, it can stay in the same state or transfer to another state. The constraint conditions and the triggers are different in different states. In the undersaturated state, the constraint conditions are

$$
\begin{aligned}
& (s_{\mathrm{w}})_l^{(n+1)} + (s_{\mathrm{o}})_l^{(n+1)} = 1, \\
& (p)_l^{(n+1)} > (p_{\mathrm{b}})_l^{(n+1)}.
\end{aligned}
\tag{4.1}
$$

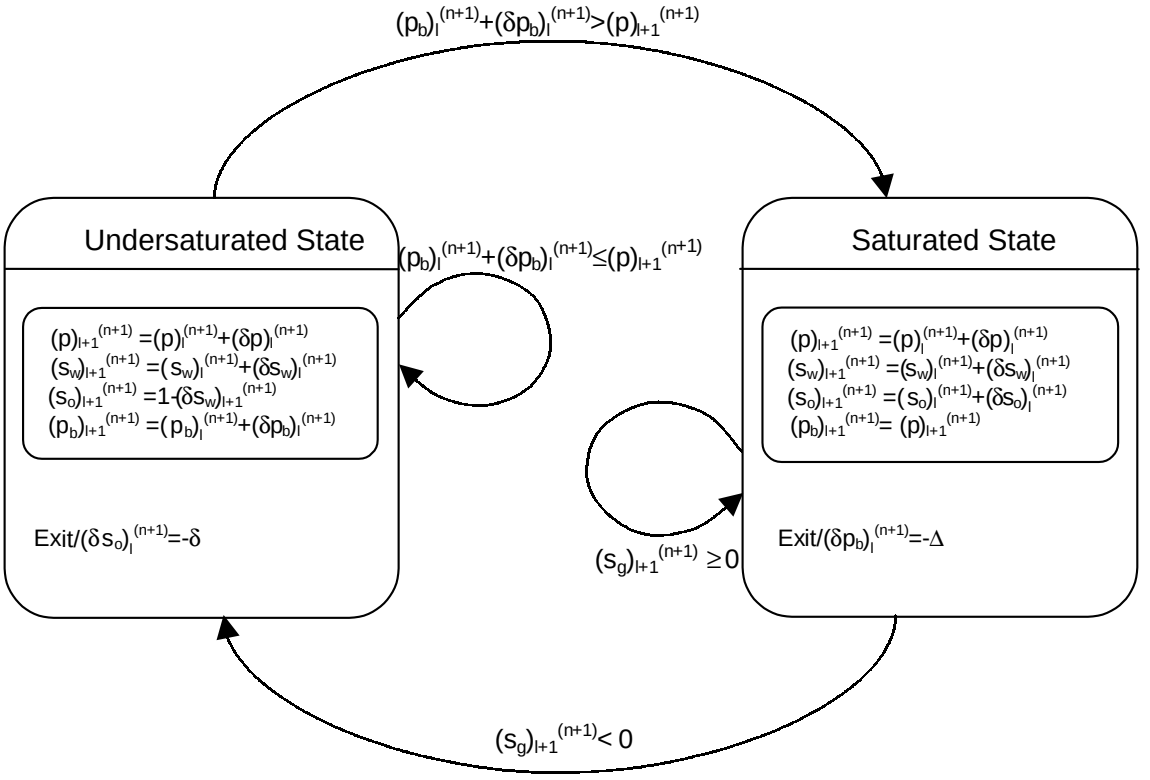

Fig. 1. State machine of the black-oil reservoir simulator.

On the other hand, in the saturated state, the constraint conditions are

$$\begin{aligned}&(s_{\mathrm{w}})_l^{(n+1)}+(s_{\mathrm{o}})_l^{(n+1)}+(s_{\mathrm{g}})_l^{(n+1)}=1,\\&(p)_l^{(n+1)}=(p_{\mathrm{b}})_l^{(n+1)}.\end{aligned}\tag{4.2}$$

The trigger that causes the transition from the undersaturated state to the saturated state is

$$(p_{\mathrm{b}})_l^{(n+1)}+(\delta p_{\mathrm{b}})_l^{(n+1)}>(p)_{l+1}^{(n+1)},\tag{4.3}$$

and the trigger causing the transition from the saturated state to the undersaturated state is

$$(s_{\mathrm{g}})_{l+1}^{(n+1)}<0.\tag{4.4}$$

To deal properly with the bubble point problem, we need to check the triggers to determine whether a location in a reservoir stays in the old state or transfers to a new state. Then, we let the unknowns satisfy the constraint conditions of the corresponding states. When the reservoir pressure at a location in a reservoir drops below the bubble point pressure, it can be found that $(p_{\mathrm{b}})_l^{(n+1)}+(\delta p_{\mathrm{b}})_l^{(n+1)}>(p)_{l+1}^{(n+1)}$, the dissolved gas will come out from the oil phase, and the oil saturation will decrease. It triggers the state to transfer from the undersaturated state to the saturated state at this location. In order to enter the new state, $(\delta s_{\mathrm{o}})_l^{(n+1)}$ is set with a small negative value so that the gas saturation is greater than zero and the dissolved gas comes out. After it enters the saturated state, the unknowns of the grid point are updated to satisfy the constraint condition (4.2). Similarly, if the reservoir pressure at a location increases high enough to have all the gas

dissolve into the oil phase, the state changes from the saturated state to the undersaturated state at this location. Correspondingly, it will be found that $(s_g)_{l+1}^{(n+1)} < 0$. This will trigger the state to transfer from the saturated state to the undersaturated state. In order to guarantee that the oil phase pressure will be greater than the bubble point pressure in the new state, $(\delta p_b)_l^{(n+1)}$ is set with a small negative value. After it enters this new state, the unknowns are updated to meet the constraint condition (4.1) of the undersaturated state.

4.2. Selection of time steps

Selecting reasonable time steps is another key to control convergence of Newton–Raphson's iterations and the computational speed of a simulation process. If time steps are too small, it will lead to too many time steps, Newton–Raphson iterations, and ORTHOMIN iterations (the linear solver used in this paper), so the computational cost increases. If time steps are too large, it will results in divergence of a Newton–Raphson iteration process, time step cutting, and wasting computational time.

To select suitable time steps, from our experimental experiences we have adopted the following empirical rules:

Rule 1. With a given maximum time step $\Delta t_{\max}$ and a given minimum time step $\Delta t_{\min}$, the time step to be determined Δt_{n+1} must satisfy that $\Delta t_{\min} \leqslant \Delta t_{n+1} \leqslant \Delta t_{\max}$.

Rule 2. In the saturated state, Δt_{n+1} is bounded by

$$\Delta t_{n+1} \leqslant \Delta t_n \min\left\{3, \frac{(\mathrm{d}P)_{\max}}{(\delta p)_{\max}^{(n)}}, \frac{(\mathrm{d}S_w)_{\max}}{(\delta s_w)_{\max}^{(n)}}, \frac{(\mathrm{d}S_g)_{\max}}{(\delta s_g)_{\max}^{(n)}}\right\}, \tag{4.5}$$

where $(\mathrm{d}P)_{\max}$, $(\mathrm{d}S_w)_{\max}$, and $(\mathrm{d}S_g)_{\max}$ are the allowable maximum values of the pressure, water saturation, and gas saturation increments, respectively, and $(\delta p)_{\max}^{(n)}$, $(\delta s_w)_{\max}^{(n)}$, $(\delta s_g)_{\max}^{(n)}$ are the maximum values of these increments at the nth time step. In the undersaturated state, (4.5) becomes

$$\Delta t_{n+1} \leqslant \Delta t_n \min\left\{3, \frac{(\mathrm{d}P)_{\max}}{(\delta p)_{\max}^{(n)}}, \frac{(\mathrm{d}S_w)_{\max}}{(\delta s_w)_{\max}^{(n)}}, \frac{(\mathrm{d}P_b)_{\max}}{(\delta p_b)_{\max}^{(n)}}\right\}, \tag{4.6}$$

where $(\mathrm{d}P_b)_{\max}$ is the allowable maximum value of the bubble point pressure increment.

Rule 3. Δt_{n+1} should guarantee that the simulation time can reach the given period times.

With these rules, the time step can automatically be selected. The choice of Δt_{n+1} also needs to take into account convergence of Newton–Raphson's iterations. If the number of Newton–Raphson's iterations is greater than a given maximum number with Δt_{n+1} selected with Rules 1–3, the determined time step may be too large and it needs to be reduced. We first cut Δt_{n+1} by $\Delta t_{n+1}/3$. Then the oil phase pressure, bubble point pressure, water saturation, and oil saturation at the nth time step are taken as the first iteration values of Newton–Raphson's iterations at the $(n+1)$th time step.

4.3. Termination of Newton–Raphson's iterations

To terminate a Newton–Raphson iteration process, some important factors must be considered. First, the iteration number must be greater than a given minimum number and smaller than a given maximum number. Second, the iteration values of the unknowns and the right-hand vectors of the linear equation systems to be solved are also used as part of the termination condition. The absolute iteration values of the increments of pressure, water saturation, oil saturation or bubble point pressure pressure, and the bottom hole pressures of wells have to be less than their respective allowable maximum limits. Also, the ratio of the infinite norm of the right-hand side vector of an LES to the maximum absolute value of the sum of the oil and gas component flow rates of perforated zones of wells have to be less than a certain given limit. Mass

balance errors are not used as one of the termination conditions of the Newton–Raphson iterations, but are monitored during a computational process. For the sequential method, the termination conditions are checked after all unknowns are obtained.

5. Numerical experiments

To test convergence, stability, accuracy, and computational speed of our sequential solution method in the treatment of large-scale simulation problems with strong heterogeneities, non-zero capillary pressures, and free gas, we use the ninth SPE CSP benchmark problem [13] and real field-scale simulation models on unstructured grids. Both saturated and undersaturated reservoirs are used to test our method and check its practical value. For the undersaturated reservoir, the nonlinearity of the governing equations caused by the high compressibility and low viscosity of the gas component is relatively weaker than that for the saturated reservoir. In addition, there is no bubble point problem for the undersaturated reservoir. Since the sequential method has lower implicity, it may be applicable to the undersaturated reservoir, not to the saturated reservoir. Therefore, it is necessary to test this method with both types of reservoirs.

5.1. An SPE benchmark problem

The benchmark problem of the ninth CSP [13] is a challenging problem due to the following reasons: First, the permeability of the reservoir is generated from geostatistical modeling, which can lead to a strong heterogeneity. Second, the water–oil capillary pressure has discontinuity when the water saturation is 0.35, which may cause divergence of the Newton–Raphson iterations. Third, the capillary pressure has a tail which does not extend to the water saturation 1.0.

We briefly state the geological and physical data; for more details on these data, see [13]. A grid of rectangular parallelepipeds for the reservoir under consideration is given in Fig. 2. Its dimensions are $7200 \times 7500 \times 359$ ft^3. The depth to cell $(1,1,1)$ of this rectangular grid is 9000 ft. It has a dip in the x-direction of 10°. The gas/oil (GOC) and water/oil contacts (WOC), respectively, locate at 8800 and 9950 ft. The reservoir has 15 layers.

In the initial state, the reservoir reaches equilibrium with an initial reservoir pressure of 3600 psia at 9035 ft and with a reservoir temperature of 100 °F. The bubble point pressure of oil is 3600 psia. At 1000 psi above the bubble point pressure P_b, B_o is 0.999 times that of B_o at P_b. The density of the stock tank oil is 0.7296 g/cc. The oil pressure gradient is approximately 0.3902 psi/ft at 3600 psia. The stock tank density of water is 1.0095 g/cc, with a water formation volume factor B_w at 3600 psia of 1.0034 RB/STB yielding a water gradient of approximately 0.436 psi/ft. The rock compressibility is 1.0×10^{-6} 1/psi. The Stone II model is used for calculating the relative permeability of the oil phase when three phases co-exist.

There are one water injector and 25 producers, whose wellbore radii are 0.50 ft. Their locations are shown in Fig. 2. The injector is perforated at layers 11–15, and the producers are perforated at layers 2–4. The water injection rate is 5000 STB/D with a maximum bottom hole pressure of 4000 psia. Initially, the oil production rate of the producers is set to 1500 STB/D. They are reduced to 100 STB/D at 300 days. Then they are raised to 1500 STB/D until the end of the simulation at 900 days. The reference depths of all wells are 9110 ft.

We compare: (a) the field oil production rate vs. time, (b) the field GOR vs. time, (c) the field water production rate vs. time, (d) the field gas production rate vs. time, (e) the water injection rate vs. time, and (f) the oil rate at well 21.

To check accuracy, stability, and convergence of our sequential method combined with the CVFA method, we also solve the same problem using the fully implicit method combined with either the CVFA or 9-point finite difference (FD) methods. We also compare our results with those generated by VIP-EXECUTIVE, which is a three-dimensional, three-phase reservoir simulator. For the CVFA method, we use

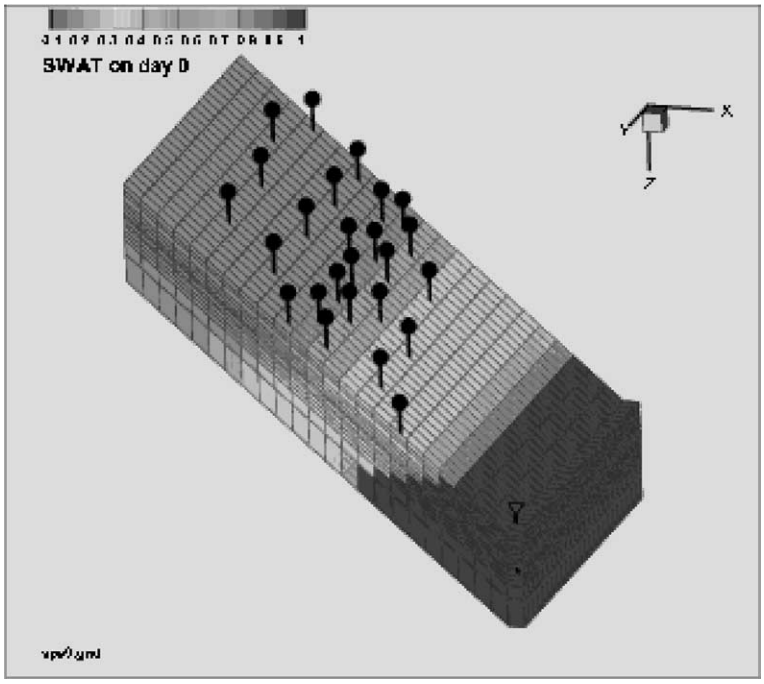

Fig. 2. The reservoir of the ninth CSP problem.

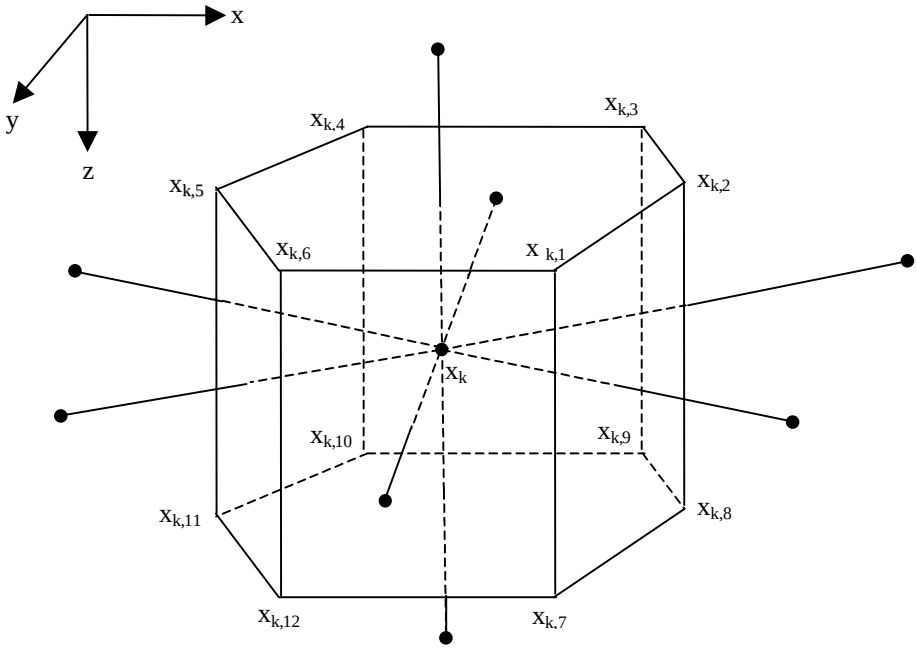

Fig. 3. A hexagonal prism.

hexagonal prisms (hexagons in the xy-plane and rectangles in the z-coordinate direction; see Fig. 3) as base grid blocks since the reservoir considered has a layer structure. The hexagons can reduce grid orientation effects [14]. In order for the wells to locate at the destination positions, the base grid blocks are adjusted with the techniques of corner point correction and local grid refinement [12]. The total number of grid blocks is 765×15, where 15 is the number of layers. The ORTHOMIN iterative algorithm [23] is used to solve the systems of linear equations, and the incomplete LU(0) factorization is used as preconditioners. The maximum saturation and pressure changes during the computational processes are set to 0.05 and 150 psi, respectively, for the fully implicit method, while the maximum saturation change for the sequential method is set to 0.02 to control convergence.

Fig. 4 is the gas saturation distribution of the first layer at 50 days, where s_g is in one of the intervals $[0, 0.02]$, $[0.02, 0.04]$, $[0.04, 0.06]$, and $[0.06, 0.08]$ from the dark to light color. The gas saturation distribution is quite unusual. It is caused by the high heterogeneity of the reservoir, whose permeability has a lognormal distribution. Figs. 5–11 are the comparative results. They show that the results of the sequential method with unstructured grids match those of the fully implicit method with unstructured grids very well. These results are closer to those from the fully implicit method combined with the FD method than to those of VIP-EXECUTIVE. The reason may be that there are minor differences between our simulator and VIP-EXECUTIVE in the treatment of the well models, linearization of conservation equations, time step control, iteration control, or type of grids used. From these plots, we see that the reservoir pressures match perfectly between the CVFA and FD methods, as shown in Fig. 10; there exist slight differences for other quantities. Since this benchmark problem has a very strong heterogeneity generated by geostatistical

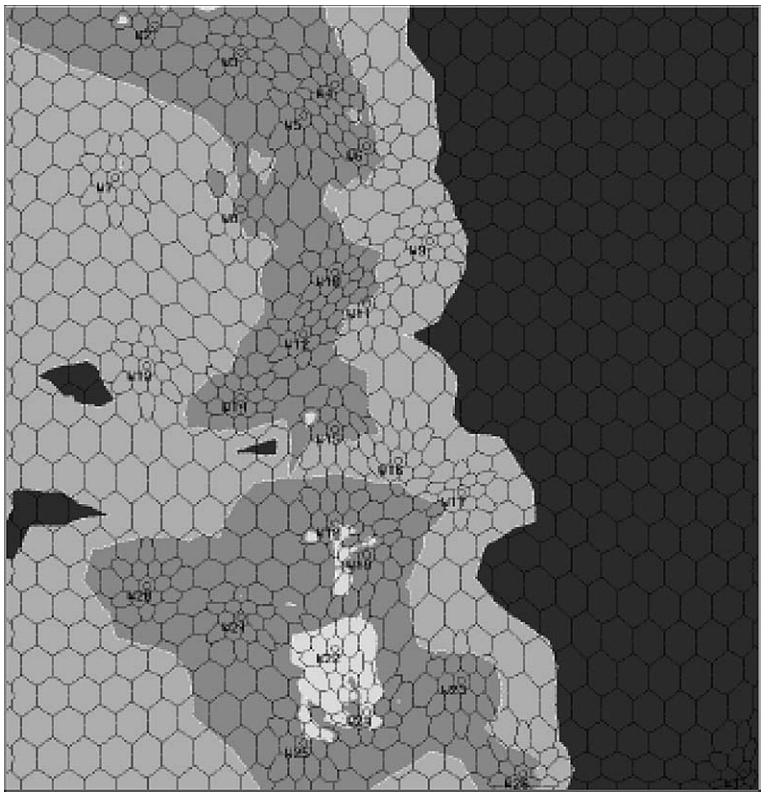

Fig. 4. Gas saturation at 50 days.

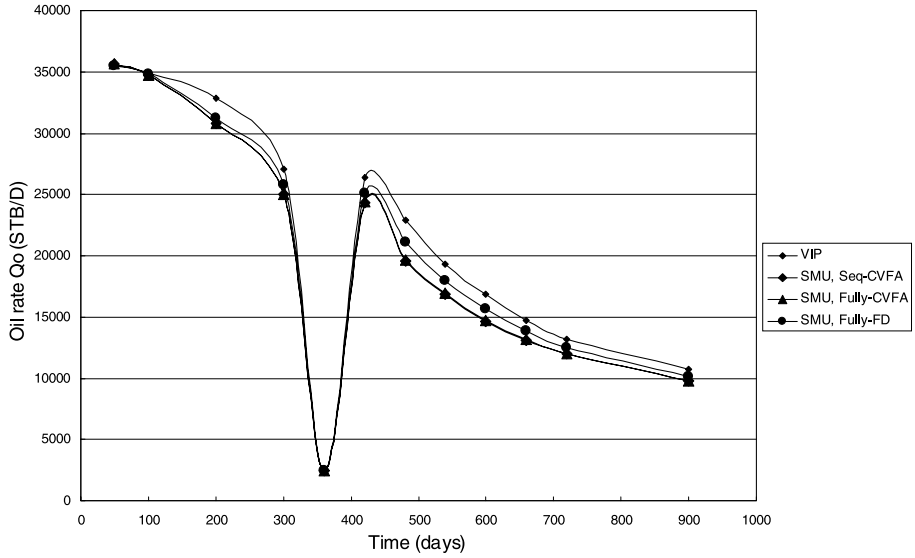

Fig. 5. Comparison of oil production rates.

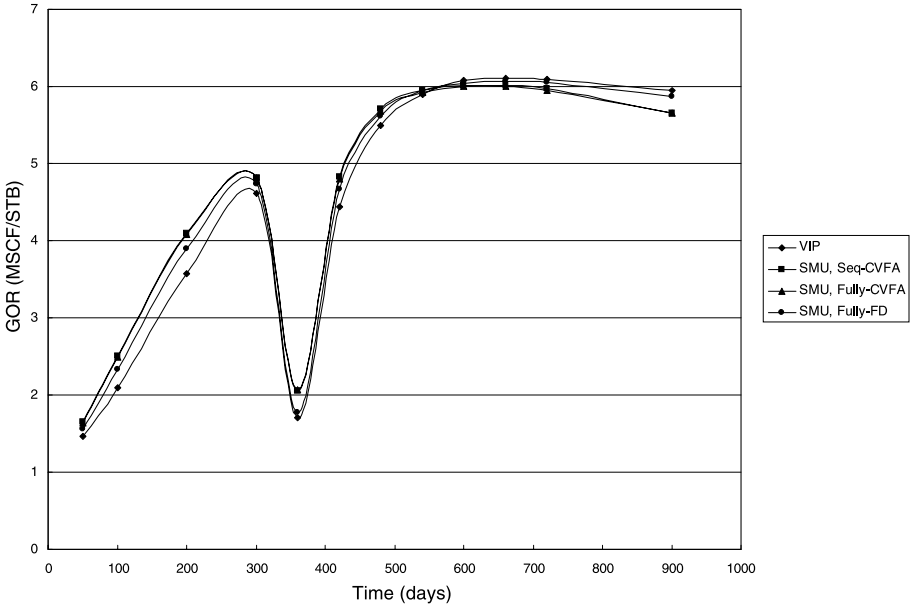

Fig. 6. Comparison of GOR vs. time.

modeling, unstructured grids can more accurately describe the heterogeneity of the reservoir, which is reflected in the production rates. Table 1 shows that the sequential method just takes 28% of the CPU time of the fully implicit method to solve the linear equations. The total CPU time is reduced by 45.5%.

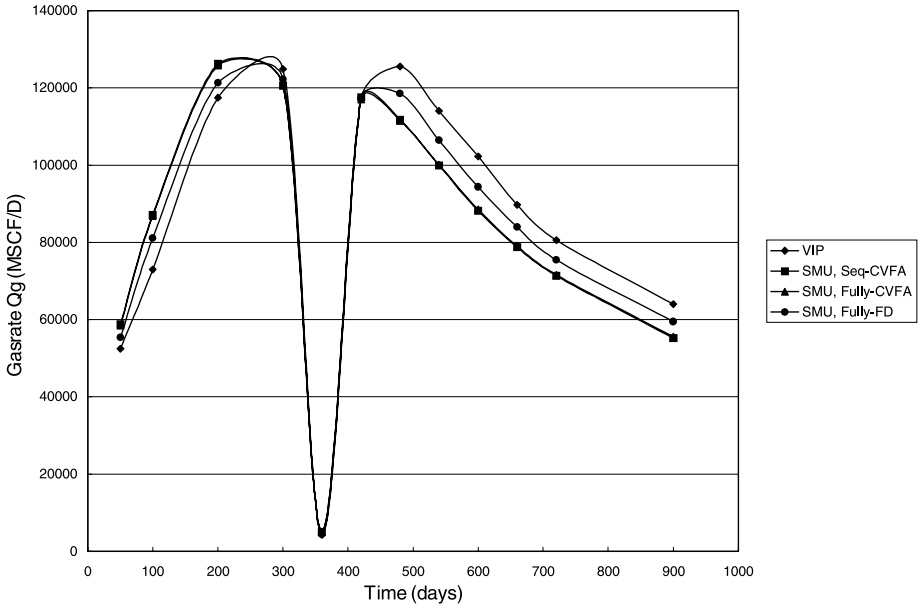

Fig. 7. Comparison of field gas rates.

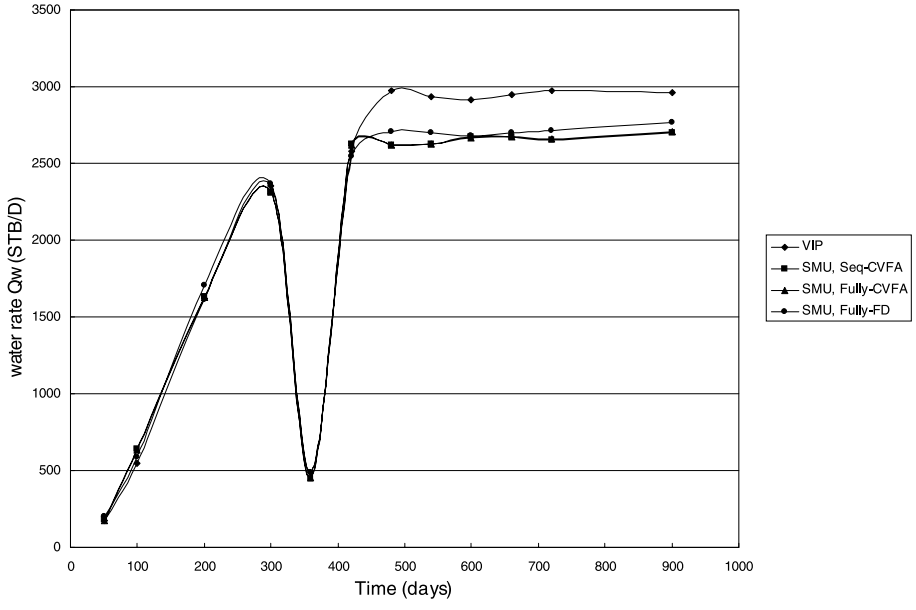

Fig. 8. Comparison of field water rates.

5.2. An undersaturated reservoir

The simulation model comes from a development scheme design for water flooding of an oil field. The dimensions of this oil field are 6890 ft × 6726 ft × 4227 ft. It has four geological layers with an irregularly

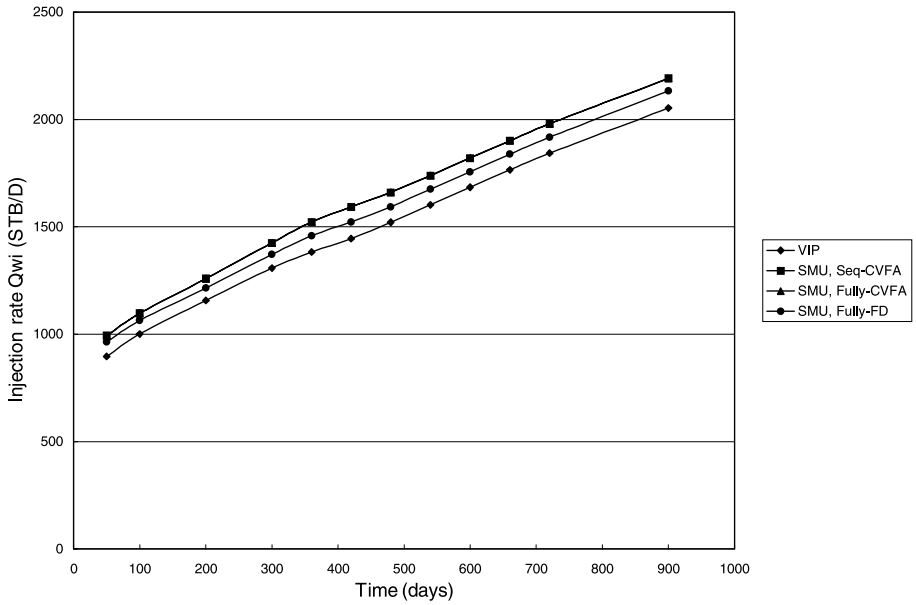

Fig. 9. Comparison of injected water rates.

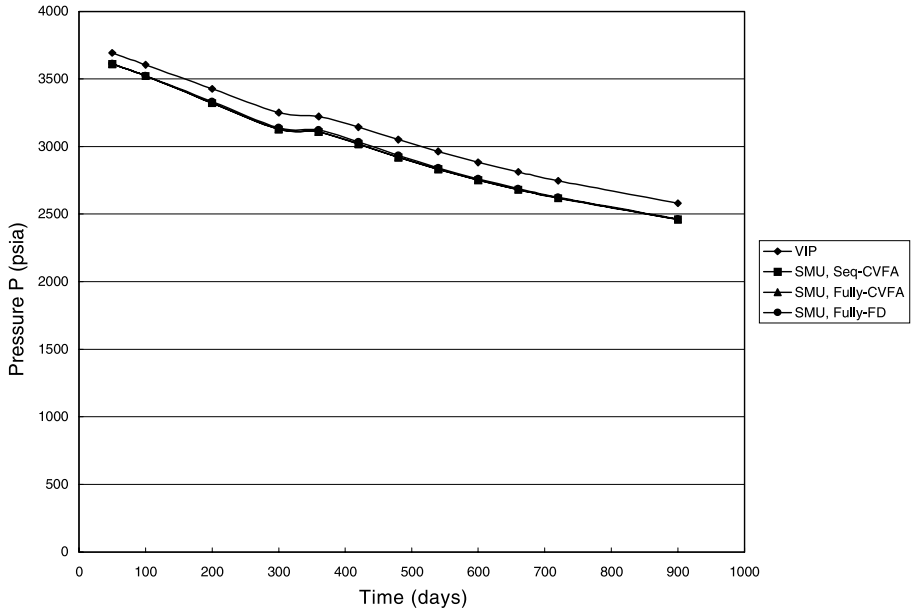

Fig. 10. Comparison of average reservoir pressure.

shaped boundary, top, and base and with reservoir temperature 165.2 °F. The absolute permeability and compressibility of rock and the thickness of the layers are variant in space. The water, oil, and oil viscosity compressibilities are 3.1×10^{-6}, 3.1×10^{-6}, and 0 psi^{-1}, respectively. The stock-tank densities for oil and

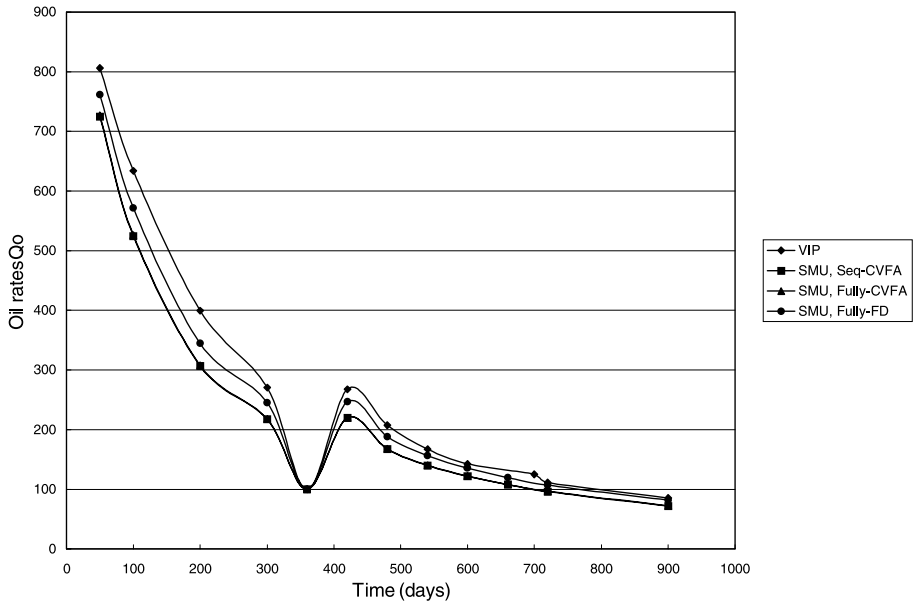

Fig. 11. Comparison of oil rates for well 21.

Table 1
Comparison of computational cost for the ninth CSP problem

Solution method	Fully implicit + CVFA	Sequential + CVFA
CPU time for LES (s)	4141.92	1174.48
Total CPU time (s)	5172.76	2819.80
Number of time steps	119	179
Number of time step cuts	0	0

water are, respectively, 60.68 and 62.43 lbm/cu ft. The gas specific gravity at the standard condition (expressed as the ratio of the molecular weight of the gas to the molecular weight of air) is 0.5615. The depths to the GOC and WOC are 3666 and 4593 ft, respectively. The reservoir is initially at capillary/gravity equilibrium with a pressure of 1624 psia at depth 3684 ft. The capillary pressures at the GOC and WOC are zero. Other PVT and rock data are given in Tables 2–4 where Z_g is the gas deviation factor, k_{row} is the

Table 2
PVT property data

P (psia)	B_o (RB/STB)	μ_o (cp)	R_{so} (SCF/STB)	B_w (RB/STB)	μ_w (cp)	Z_g	μ_g (cp)
87.02	1.0057	52.8	6.74	1.022	0.42	0.993	0.0151
435.11	1.0208	37.6	9.19	1.022	0.42	0.966	0.0141
870.23	1.0415	26.3	83.66	1.022	0.42	0.936	0.0132
1305.34	1.0632	19.7	130.25	1.022	0.42	0.913	0.0141
1624.42	1.0795	15.5	165.63	1.022	0.42	0.898	0.0151

Table 3
Saturation function data for water/oil

s_w	K_{rw}	K_{row}	p_{cow} (psi)
0.2400	0.000	1.000	2.4656
0.3050	0.001	0.809	1.1603
0.3266	0.002	0.707	0.8702
0.3483	0.004	0.606	0.5802
0.3699	0.007	0.513	0.3916
0.3915	0.010	0.421	0.2321
0.4131	0.014	0.349	0.1450
0.5000	0.037	0.260	0.0725
0.6000	0.087	0.200	0.0435
0.7000	0.155	0.150	0.0232
0.8000	0.230	0.100	0.0000
0.9000	0.400	0.000	0.0000
1.0000	1.000	0.000	0.0000

Table 4
Saturation function data for gas/oil

s_g	K_{rg}	K_{rog}	p_{cgo} (psi)
0.00	0.000	1.0000	0.0
0.04	0.000	0.4910	0.0
0.10	0.001	0.2990	0.0
0.20	0.003	0.1200	0.0
0.22	0.007	0.1030	0.0
0.29	0.015	0.0400	0.0
0.33	0.030	0.0210	0.0
0.37	0.065	0.0087	0.0
0.40	0.131	0.0021	0.0
0.46	0.250	0.0000	0.0
0.76	1.000	0.0000	0.0

relative permeability the oil phase for an oil–water system, and k_{rog} is the relative permeability of the oil phase for a gas–oil system.

There are 50 oil production wells and 20 water injection wells. They perforate all the layers (above the WOC). The wellbore radius of each well is 0.25 ft. The well controls can be the bottom hole pressure, water injection rate, oil production rate, and liquid production rate controls with a water cut limit of 0.95.

Due to the layer structure in the vertical direction of this reservoir, we again divide its domain into hexagonal prisms, as seen in Fig. 3. The number of control volumes is 2088×4. The CVFA method is used for the discretization of the governing equations. We run the simulator with $(\mathrm{d}P)_{\max} = 300$ psia, $(\mathrm{d}S_w)_{\max} = 0.05$, and $(\mathrm{d}P_b)_{\max} = 300$ psia (see Section 4.2) and stop running at 4740 days, using the fully implicit and sequential solution methods. Fig. 12 is the water saturation for the fourth layer. Figs. 13–15 are the plots of the oil production rate, water cut, and oil recovery. The comparative results of memory and computational cost for these two solution methods are listed in Table 5. Figs. 13–15 show that the numerical results obtained from these two methods match very well. Table 5 shows that the sequential method uses as little as 20.01% of the memory for the fully implicit method to solve the LESs, which is due to the reduction of the size of the LESs. The sequential method spends just 12.06% of CPU time used by the fully implicit method to solve the LESs. The total CPU time spent by the sequential method is only 23.89% of that taken by the fully implicit method.

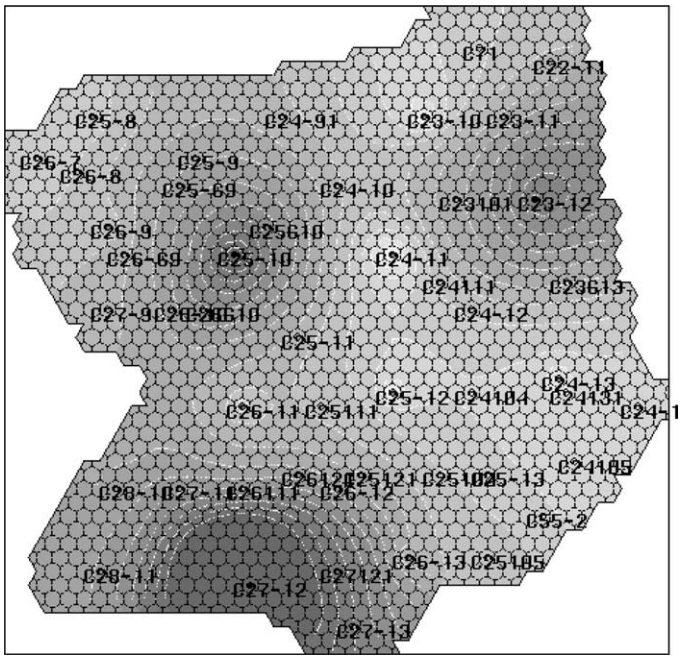

Fig. 12. Water saturation for an undersaturated oil field.

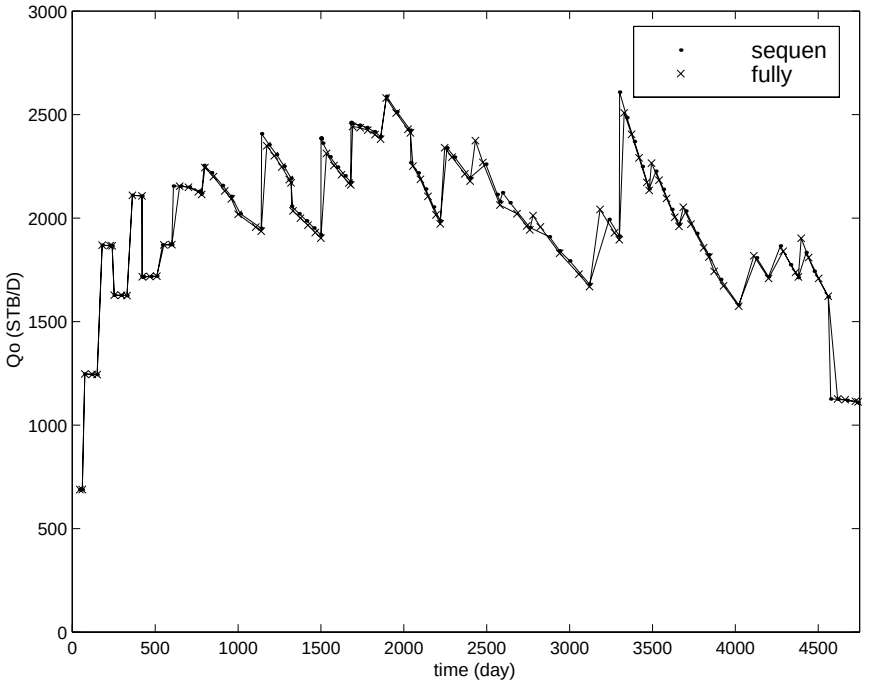

Fig. 13. Oil production rate of an undersaturated oil field.

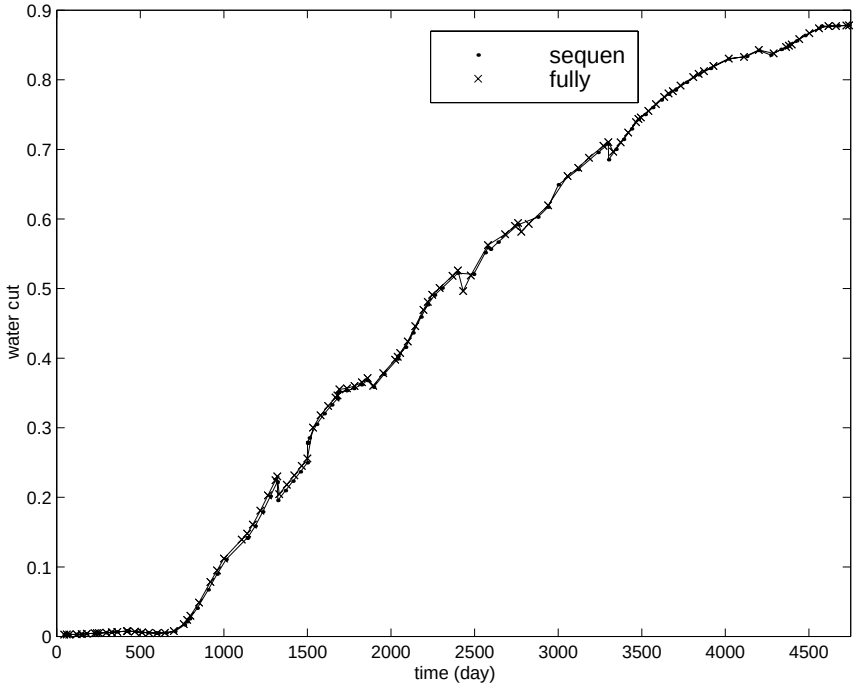

Fig. 14. Water cut of an undersaturated oil field.

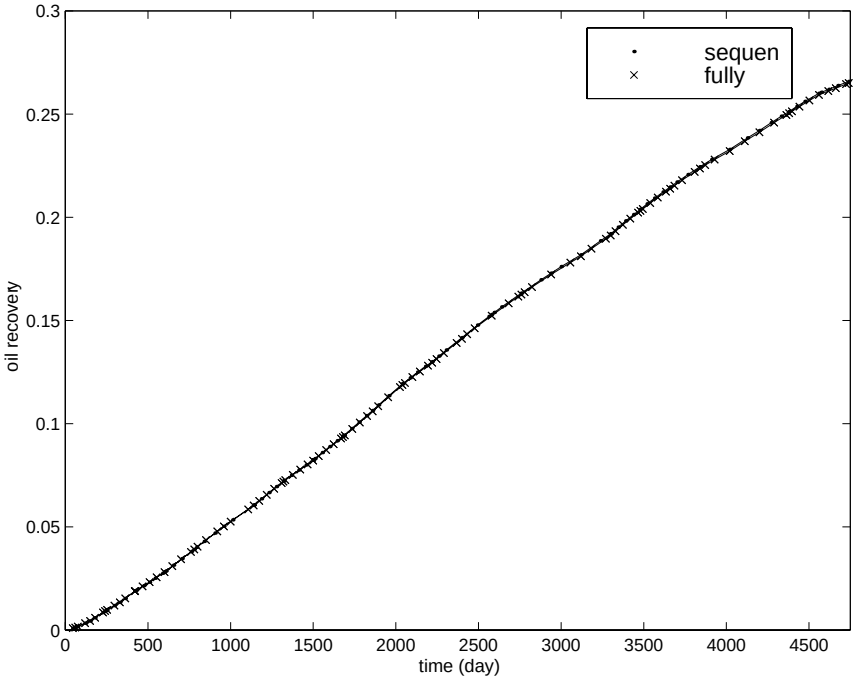

Fig. 15. Oil recovery of an undersaturated oil field.

Table 5
Comparison of computational cost and memory for an undersaturated reservoir

Solution method	Fully implicit	Sequential
CPU time for solution of LES (s)	2790.80	336.55
Total CPU time for simulation (s)	3340.19	798.05
Number of time steps	30	30
Number of time step cuts	0	0
Memory for LES solver (MB)	18.099264	3.621892
Total memory (MB)	26.326132	11.84876

The reason for reducing the computational cost for reservoir simulation using the sequential method can be seen as follows. From Table 5, we find that 83.55% of the computational cost is spent on solving the LESs and other calculations just take 549.39 s for the fully implicit method. But for the sequential method, only 42.17% of the total CPU time is spent on solving the LESs, and the CPU time taken by other calculations is only 87.89 s less than that used by the fully implicit method. Therefore, the primary reason that the sequential method is faster than the fully implicit method is that the sequential method can greatly reduce the cost to solve the LESs. Also, we note that the sequential method requires less memory.

5.3. A saturated reservoir

Two cases are designed to check the validity of the sequential method for simulation of a saturated reservoir. For the first case, we simply raise the initial bubble point pressure of the oil field described in the previous section to 1642 psia so that we initially have a saturated reservoir. For the second case, we change a production well, which is located at an upper part of this field and is shut down at 510 days, into a gas injection well to improve oil recovery with an upper limit of GOR 0.2 MSCF/RB after 600 days. Its injection rate is 500 MSCF/day.

For these two cases, we run the simulator with the same control parameters as those given in the previous section, using both the fully implicit and sequential methods. The computational results are shown in Figs. 16–24. The computational cost and memory usage are stated in Tables 6 and 7. From Figs. 16–19, we see that the oil production rate, GOR, water cut, and oil recovery obtained from these two methods match very well for the first case. In this case, the total CPU time taken by the sequential method increases to 34.60% of that for the fully implicit method. However, for the second case, although the oil production rate, water cut, and oil recovery from the sequential method still match those from the fully implicit method, there is a deviation between the GORs for these two methods after the 3700 days (see Fig. 22). Also, in this case, the CPU time for the sequential method to solve the LESs is 18.22% of that for the fully implicit method, and the total computational time for the former becomes 40.78% of that for the latter. The number of Newton–Raphson's iterations taken by the sequential method is 10 more than that for the fully implicit method.

The nonlinearity caused by the free gas and the bubble point problem is the main reason for these phenomena. The free gas has a large compressibility, compared with water and oil. It makes a great contribution to the flow term of the governing equation of the gas component for a grid point of a reservoir in the saturated state. If the contribution is ignored by the sequential method to obtain a pressure equation, it will introduce a large approximation error to the resulting pressure equation. Especially, this may give a wrong direction in which the Newton–Raphson iteration converges at a bubble point. For a saturated reservoir, the state at a location may transfer from the saturated state to the undersaturated state. At a bubble point, if the pressure is not correct, wrong PVT data of oil will be used and a Newton–Raphson iteration will approach a wrong value. For the first case, the free gas comes from the dissolved gas in the reservoir, and the GOR is just 0.15, which is rather low. The nonlinearity

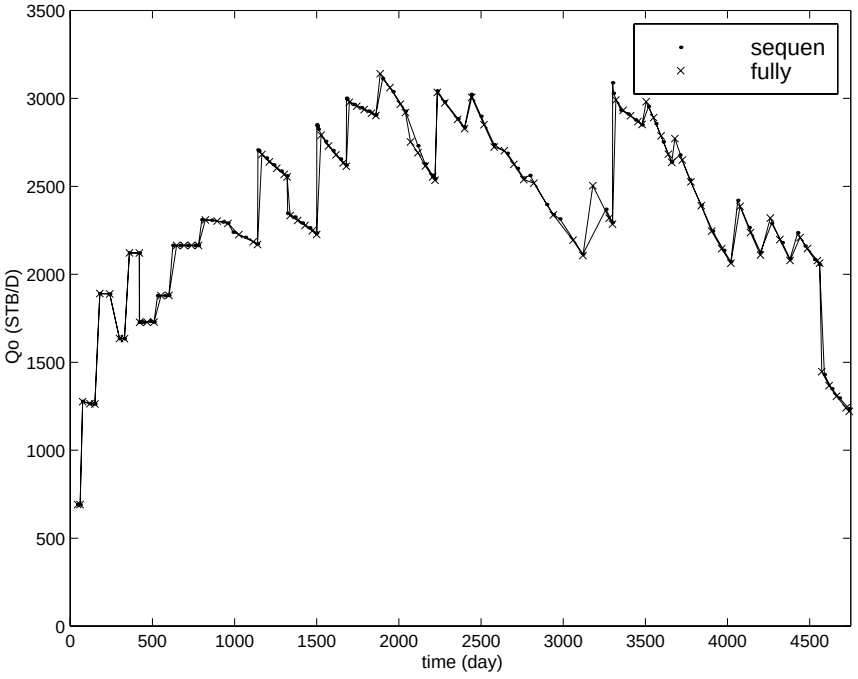

Fig. 16. Oil production rate for the water flooding of a saturated field.

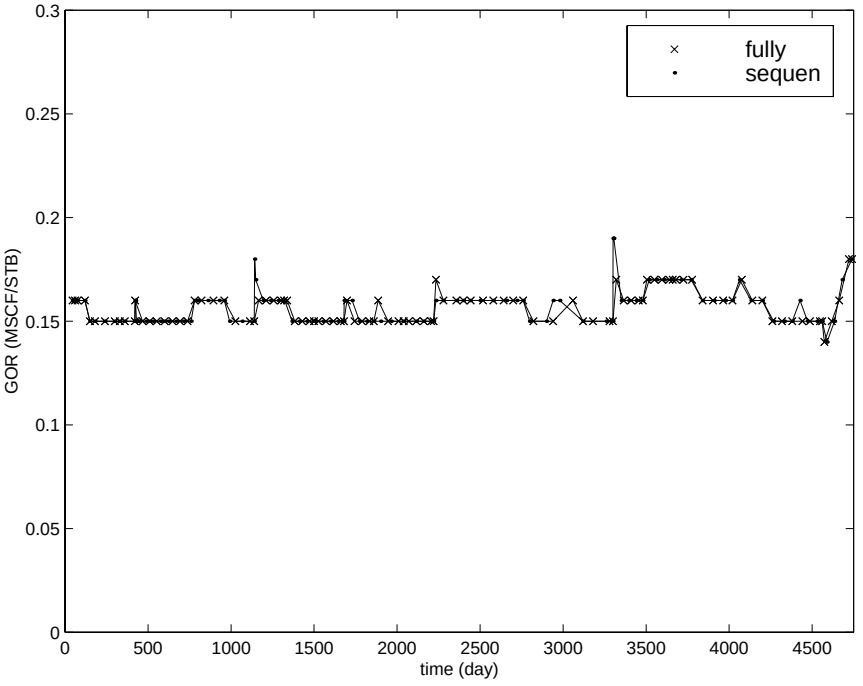

Fig. 17. GOR for the water flooding of a saturated field.

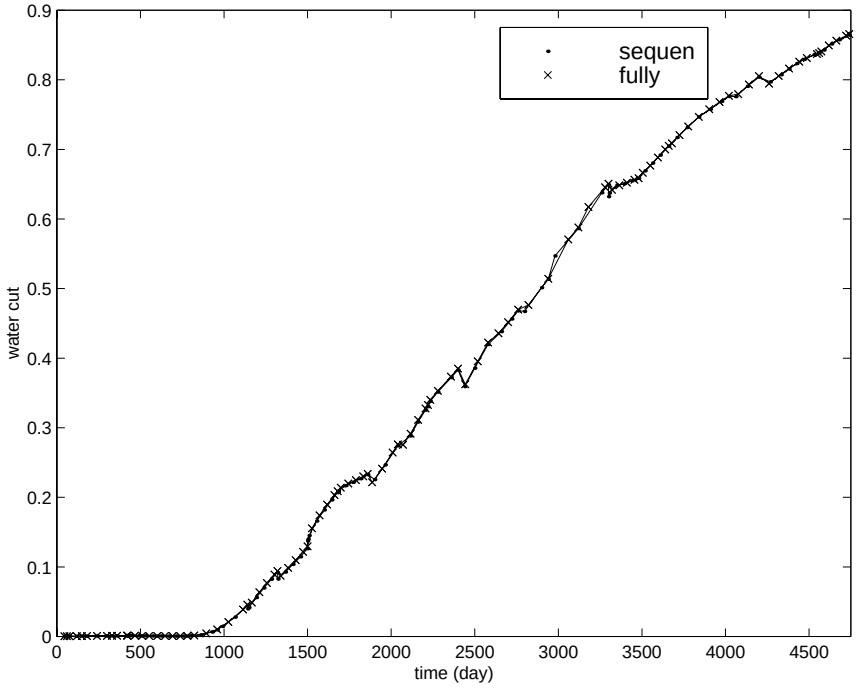

Fig. 18. Water cut for the water flooding of a saturated field.

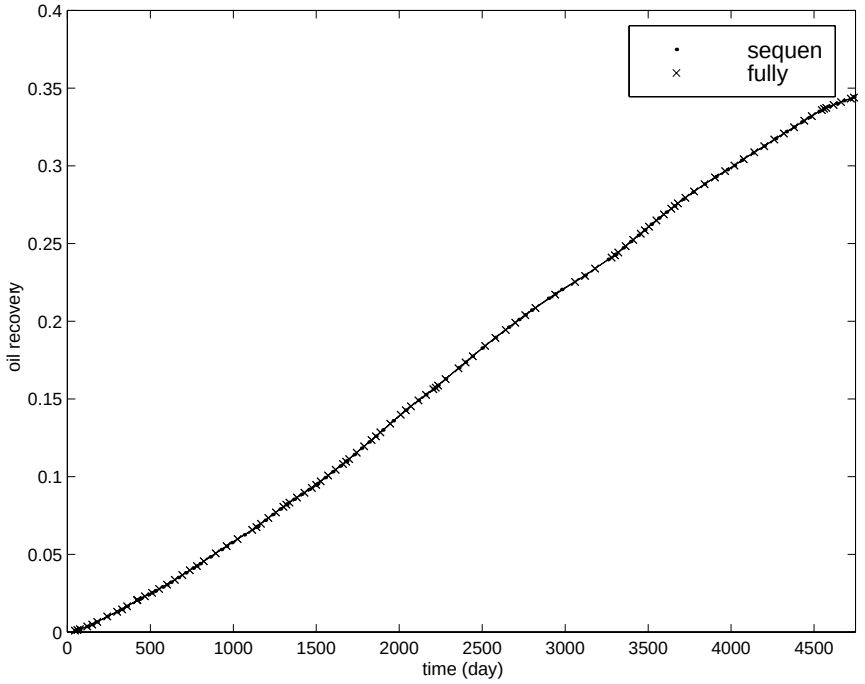

Fig. 19. Oil recovery for the water flooding of a saturated field.

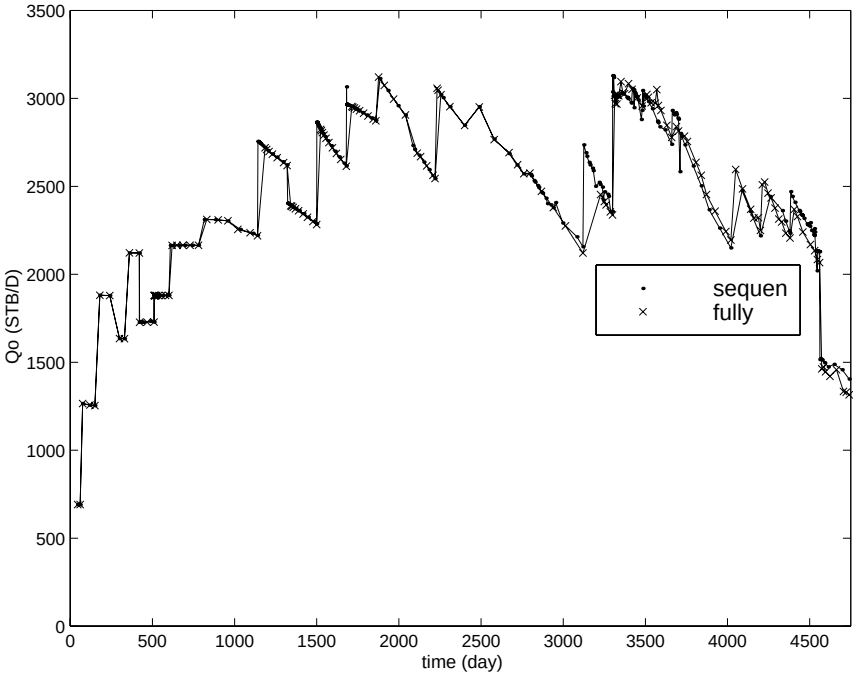

Fig. 20. Oil production rate for the gas injection of a saturated field.

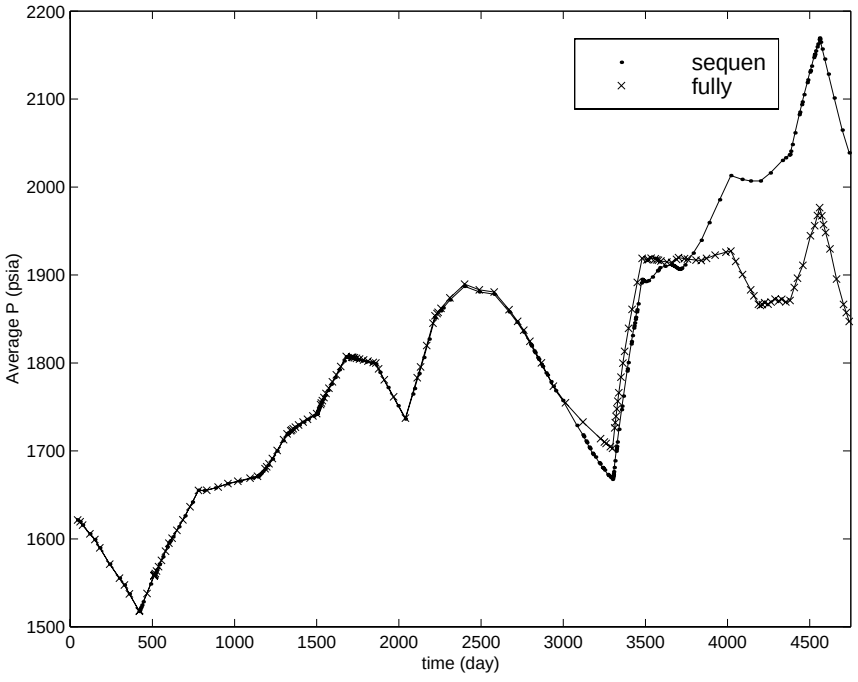

Fig. 21. Average reservoir pressure for the gas injection of a saturated field.

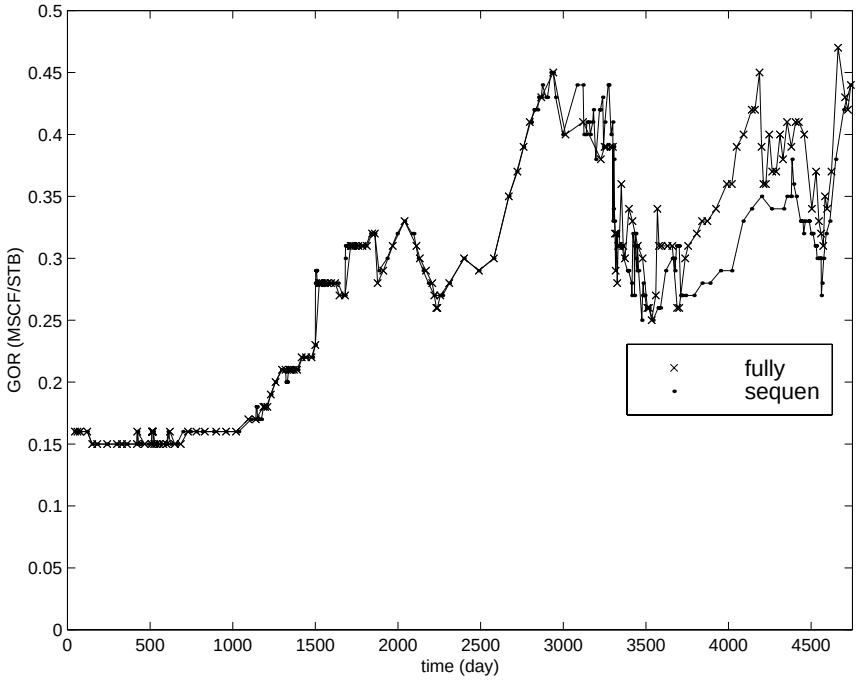

Fig. 22. GOR for the gas injection of a saturated field.

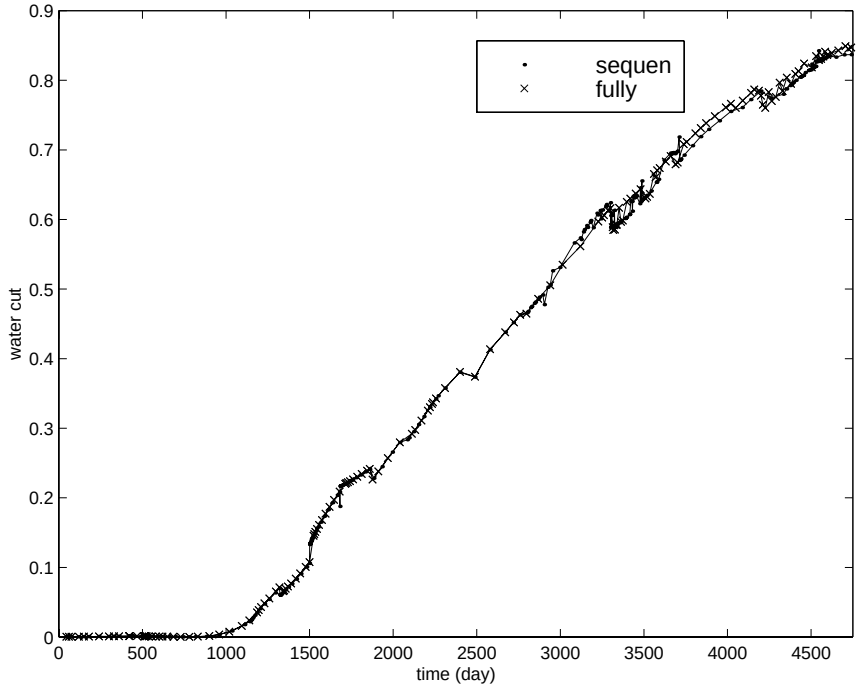

Fig. 23. Water cut for the gas injection of a saturated field.

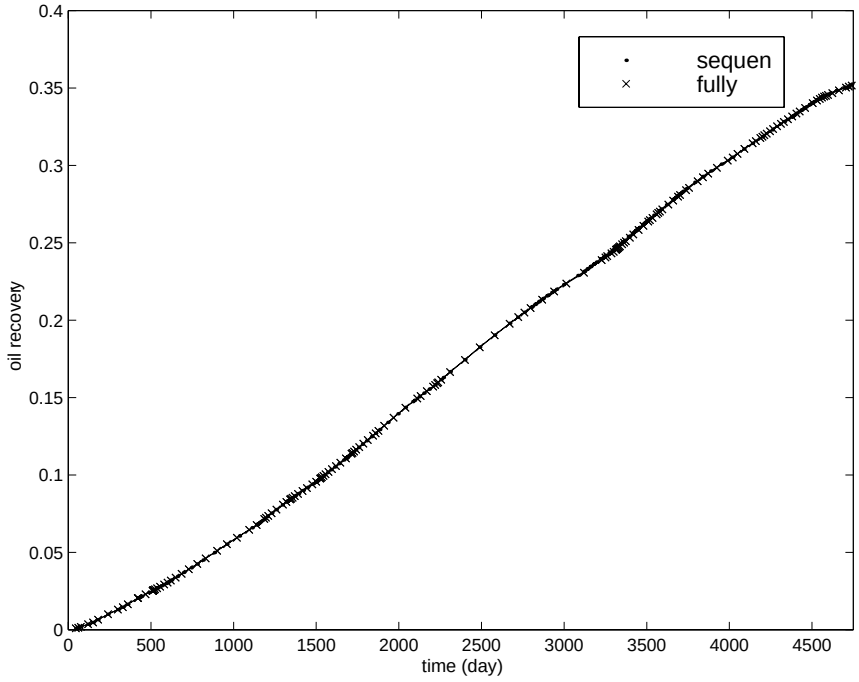

Fig. 24. Oil recovery for the gas injection of a saturated field.

Table 6
Comparison of computational cost and memory for the water flooding of a saturated field

Solution method	Fully implicit	Sequential
CPU time for solution of LES (s)	2485.88	518.58
Total CPU time for simulation (s)	3067.10	1061.09
Number of time steps	30	30
Number of time step cuts	0	0
Number of Newton–Raphson iterations	104	146
Memory for LES solver (MB)	18.099264	3.621892
Total memory (MB)	26.326132	11.84876

Table 7
Comparison of computational cost and memory for gas injection of a saturated field

Solution method	Fully implicit	Sequential
CPU time for solution of LES (s)	5008.60	912.93
Total CPU time for simulation (s)	5869.08	2393.66
Number of time steps	30	30
Number of time step cuts	0	0
Number of Newton–Raphson iterations	137	147
Memory for LES solver (MB)	18.099264	3.621892
Total memory (MB)	26.326132	11.84876

caused by the free gas is weak. The approximation error for the pressure equation introduced by the sequential method is small. Therefore, its convergence rate is high. However, for the second case, a great amount of free gas is injected into the reservoir. The nonlinearity caused by the free gas is strong. After

3700 days, the oil production rate of the field drops quickly, the pressure obtained from the sequential method is higher than the real value because of ignoring the nonlinearity term caused by the free gas and water (see Fig. 21), and at this pressure more free gas dissolves into oil and leads to the GOR deviating from its true value.

6. Conclusions

We have applied the sequential solution method to the black-oil reservoir simulation with unstructured grids. The CVFA method has been employed for the discretization of the governing equations of the black oil model. Field-scale simulation models of oil reservoirs have been used to test this solution method for both the saturated and undersaturated states of these reservoirs.

The numerical experiment results show that the sequential method is convergent and stable for an undersaturated reservoir, and the results in Section 5.1 match those of VIP-EXECUTIVE very well. During a Newton–Raphson iteration process, no time step cut occurs. It can reduce computational cost and memory by 87.94% and 79.99%, respectively, of those for the fully implicit method to solve the LESs of the model in Section 5.2. For a saturated reservoir, the convergence and accuracy of the sequential method depends on whether free gas is injected. If there is no gas injection, this solution method is still convergent and accurate and it can reduce the total computational cost by 65.40% of that for the fully implicit method for the first case in Section 5.3. But, in the case of gas injection, the pressure and GOR obtained from this method may deviate from those obtained from the fully implicit method, even though it is convergent. In summary, the sequential solution method can greatly reduce computational cost and save memory of reservoir simulation with unstructured grids by reducing the size of the LESs to be solved for undersaturated reservoirs.

Acknowledgements

The authors would like to thank Dr. John E. Killough for generously supplying the input and output data of VIP-EXECUTIVE for us to test our new solution method. Also, the authors wish to thank a referee for many helpful comments and suggestions in this paper.

Appendix A. Linearization of the governing equations and well control equations

In this section we carry out the linearization of the governing equations of the black-oil model using Newton–Raphson's procedure. Again, the unknown variables are different under the different states of a reservoir, so we discuss them separately,

A.1. Undersaturated state

Under the undersaturated state, the unknowns are $p = p_o$, s_w, and p_b. After substitution of Eq. (2.4) into Eqs. (2.1)–(2.3), the integral forms of the resulting equations on each control volume V_i, $i = 1, 2, \ldots, N$, can be discretized by the backward Euler difference method in time and linearized by the Newton–Raphson procedure as follows. Set, for $y = w, o$,

$$H_y^1 = \frac{KK_{ry}}{\mu_y}\frac{\rho_{YS}}{B_y} + KK_{ry}\frac{\partial}{\partial p}\left(\frac{\rho_{YS}}{\mu_y B_y}\right)\delta p + \frac{K\rho_{YS}}{\mu_y B_y}\frac{\partial K_{ry}}{\partial s_w}\delta s_w,$$

$$H_y^2 = \frac{KK_{ry}}{\mu_y}\frac{\rho_{YS}}{B_y}\nabla(\delta p),$$

$$H_{y,k,m}^3 = q_{y,k,m} + \frac{\mu_y B_y}{\rho_{YS}}q_{y,k,m}\frac{\partial}{\partial p}\left(\frac{\rho_{YS}}{\mu_y B_y}\right)\delta p + \frac{q_{y,k,m}}{K_{ry}}\frac{\partial K_{ry}}{\partial s_w}\delta s_w + \mathrm{WI}_{k,m}\frac{K_{ry}\rho_{WS}}{\mu_y B_y}(\delta p_{bh,k} - \delta p),$$

$$H_{y,l}^{4,n+1} = \left(\phi\frac{\rho_{YS}}{B_y}s_y\right)_l^{(n+1)} - \left(\phi\frac{\rho_{YS}}{B_y}s_y\right)^{(n)} + \left[c_r\phi_a\frac{\rho_{YS}}{B_y}s_y + \phi s_y\frac{\partial}{\partial p}\left(\frac{\rho_{YS}}{B_y}\right)\right]_l^{(n+1)}(\delta p)_l^{(n+1)},$$

where n indicates the nth time step and l represents the lth iteration of the Newton–Raphson procedure. Then, for the water component, we have

$$\int_{\partial V_i}\{H_w^1\}_l^{(n+1)}(\nabla\Phi_w)_l^{(n+1)}\cdot\mathbf{n}\,dA + \int_{\partial V_i}[H_w^2]_l^{(n+1)}\cdot\mathbf{n}\,dA - \int_{\partial V_i}\left[\frac{KK_{rw}}{\mu_w}\frac{\rho_{WS}}{B_w}\nabla\left(\frac{\partial p_{cow}}{\partial s_w}\delta s_w\right)\right]_l^{(n+1)}\cdot\mathbf{n}\,dA + \sum_{k=1}^{N_w}\sum_{m=1}^{M_{w,k}}\int_{V_i}\left\{H_{w,k,m}^3\right\}_l^{(n+1)}\delta_{k,m}\,d\mathbf{x} = \frac{V_i}{\Delta t_n}\left\{H_{w,l}^{4,n+1} + \left(\phi\frac{\rho_{WS}}{B_w}\right)_l^{(n+1)}(\delta s_w)_l^{(n+1)}\right\}_{\mathbf{x}=\mathbf{x}_i},$$

for the oil component,

$$\int_{\partial V_i}\left\{H_o^1 + KK_{ro}\frac{\partial}{\partial p_b}\left(\frac{\rho_{OS}}{\mu_o B_o}\right)\delta p_b\right\}_l^{(n+1)}(\nabla\Phi_o)_l^{(n+1)}\cdot\mathbf{n}\,dA + \int_{\partial V_i}\left[H_o^2\right]_l^{(n+1)}\cdot\mathbf{n}\,dA + \sum_{k=1}^{N_w}\sum_{m=1}^{M_{w,k}}\int_{V_i}\left\{H_{o,k,m}^3 + \frac{\mu_o B_o}{\rho_{OS}}q_{o,k,m}\frac{\partial}{\partial p_b}\left(\frac{\rho_{OS}}{\mu_o B_o}\right)\delta p_b\right\}_l^{(n+1)}\delta_{k,m}\,d\mathbf{x} = \frac{V_i}{\Delta t_n}\left\{H_{o,l}^{4,n+1} + \left[\phi s_o\frac{\partial}{\partial p_b}\left(\frac{\rho_{OS}}{B_o}\right)\right]_l^{(n+1)}(\delta p_b)_l^{(n+1)} - \left(\phi\frac{\rho_{OS}}{B_o}\right)_l^{(n+1)}(\delta s_w)_l^{(n+1)}\right\}_{\mathbf{x}=\mathbf{x}_i},$$

and, for the gas component,

$$\int_{\partial V_i}\left\{\frac{KK_{ro}}{\mu_o}\frac{R_{so}\rho_{GS}}{B_o} + KK_{ro}\frac{\partial}{\partial p}\left(\frac{R_{so}\rho_{GS}}{\mu_o B_o}\right)\delta p + \frac{KR_{so}\rho_{GS}}{\mu_o B_o}\frac{\partial K_{ro}}{\partial s_w}\delta s_w + KK_{ro}\frac{\partial}{\partial p_b}\left(\frac{R_{so}\rho_{GS}}{\mu_o B_o}\right)\delta p_b\right\}_l^{(n+1)}(\nabla\Phi_o)_l^{(n+1)}\cdot\mathbf{n}\,dA + \int_{\partial V_i}\left[\frac{KK_{ro}}{\mu_o}\frac{R_{so}\rho_{GS}}{B_o}\nabla(\delta p)\right]_l^{(n+1)}\cdot\mathbf{n}\,dA + \sum_{k=1}^{N_w}\sum_{m=1}^{M_{w,k}}\int_{V_i}\left\{q_{o,k,m}^G + \frac{\mu_o B_o}{R_{so}\rho_{GS}}q_{o,k,m}^G\frac{\partial}{\partial p}\left(\frac{R_{so}\rho_{GS}}{\mu_o B_o}\right)\delta p + \frac{q_{o,k,m}^G}{K_{ro}}\frac{\partial K_{ro}}{\partial s_w}\delta s_w + \frac{\mu_o B_o}{R_{so}\rho_{GS}}q_{o,k,m}^G\frac{\partial}{\partial p_b}\left(\frac{R_{so}\rho_{GS}}{\mu_o B_o}\right)\delta p_b + \mathrm{WI}_{k,m}\frac{K_{ro}R_{so}\rho_{GS}}{\mu_o B_o}(\delta p_{bh,k} - \delta p)\right\}_l^{(n+1)}\delta_{k,m}\,d\mathbf{x} = \frac{V_i}{\Delta t_n}\left\{\left(\phi\frac{R_{so}\rho_{GS}}{B_o}s_o\right)_l^{(n+1)} - \left(\phi\frac{R_{so}\rho_{GS}}{B_o}s_o\right)^{(n)} + \left[c_r\phi_a\frac{R_{so}\rho_{GS}}{B_o}s_o + \phi s_o\frac{\partial}{\partial p}\left(\frac{R_{so}\rho_{GS}}{B_o}\right)\right]_l^{(n+1)}(\delta p)_l^{(n+1)} - \left(\phi\frac{R_{so}\rho_{GS}}{B_o}\right)_l^{(n+1)}(\delta s_w)_l^{(n+1)} + \left[\phi s_o\frac{\partial}{\partial p_b}\left(\frac{R_{so}\rho_{GS}}{B_o}\right)\right]_l^{(n+1)}(\delta p_b)_l^{(n+1)}\right\}_{\mathbf{x}=\mathbf{x}_i}.$$

Under this state, the well controls are implicitly treated as follows. For a bottom hole pressure control of a kth well, the bottom pressure is constant:

$$\delta p_{\mathrm{bh},k} = 0.$$

For the water injection rate control of a kth well, by (2.8), the well constraint can be treated as

$$\sum_{m=1}^{M_{\mathrm{w},k}} \int_{V_{k,m}} \left\{ \mathrm{WI}_{k,m} \frac{K_{\mathrm{rwmax}} \rho_{\mathrm{WS}}}{\mu_{\mathrm{w}} B_{\mathrm{w}}} (\delta p_{\mathrm{bh},k} - \delta p) + q_{\mathrm{wk},m} \left[1 + \frac{\mu_{\mathrm{w}} B_{\mathrm{w}}}{\rho_{\mathrm{WS}}} \frac{\partial}{\partial p} \left(\frac{\rho_{\mathrm{WS}}}{\mu_{\mathrm{w}} B_{\mathrm{w}}} \right) \delta p + \frac{1}{K_{\mathrm{rw}}} \frac{\partial K_{\mathrm{rw}}}{\partial s_{\mathrm{w}}} \delta s_{\mathrm{w}} \right] \right\}_l^{(n+1)} \delta_{k,m} \, \mathrm{d}\mathbf{x} = Q_{\mathrm{W},k}.$$

Similarly, for the oil production rate control of a kth well, the well constraint has the form

$$\sum_{m=1}^{M_{\mathrm{w},k}} \int_{V_{k,m}} \left\{ \mathrm{WI}_{k,m} \frac{K_{\mathrm{ro}} \rho_{\mathrm{OS}}}{\mu_{\mathrm{o}} B_{\mathrm{o}}} (\delta p_{\mathrm{bh},k} - \delta p) + q_{ok,m} \left[1 + \frac{\mu_{\mathrm{o}} B_{\mathrm{o}}}{\rho_{\mathrm{OS}}} \frac{\partial}{\partial p} \left(\frac{\rho_{\mathrm{OS}}}{\mu_{\mathrm{o}} B_{\mathrm{o}}} \right) \delta p + \frac{1}{K_{\mathrm{ro}}} \frac{\partial K_{\mathrm{ro}}}{\partial s_{\mathrm{w}}} \delta s_{\mathrm{w}} + \frac{\mu_{\mathrm{o}} B_{\mathrm{o}}}{\rho_{\mathrm{OS}}} \frac{\partial}{\partial p_{\mathrm{b}}} \left(\frac{\rho_{\mathrm{OS}}}{\mu_{\mathrm{o}} B_{\mathrm{o}}} \right) \delta p_{\mathrm{b}} \right] \right\}_l^{(n+1)} \delta_{k,m} \, \mathrm{d}\mathbf{x} = Q_{\mathrm{O},k},$$

and for the liquid flow rate control of production of a kth well,

$$\begin{aligned} \sum_{m=1}^{M_{\mathrm{w},k}} \int_{V_{k,m}} & \left\{ \mathrm{WI}_{k,m} \frac{K_{\mathrm{rw}} \rho_{\mathrm{WS}}}{\mu_{\mathrm{w}} B_{\mathrm{w}}} (\delta p_{\mathrm{bh},k} - \delta p) + q_{\mathrm{wk},m} \left[1 + \frac{\mu_{\mathrm{w}} B_{\mathrm{w}}}{\rho_{\mathrm{WS}}} \frac{\partial}{\partial p} \left(\frac{\rho_{\mathrm{WS}}}{\mu_{\mathrm{w}} B_{\mathrm{w}}} \right) \delta p + \frac{1}{K_{\mathrm{rw}}} \frac{\partial K_{\mathrm{rw}}}{\partial s_{\mathrm{w}}} \delta s_{\mathrm{w}} \right] \right. \\ & + \mathrm{WI}_{k,m} \frac{K_{\mathrm{ro}} \rho_{\mathrm{OS}}}{\mu_{\mathrm{o}} B_{\mathrm{o}}} (\delta p_{\mathrm{bh},k} - \delta p) + q_{ok,m} \left[1 + \frac{\mu_{\mathrm{o}} B_{\mathrm{o}}}{\rho_{\mathrm{OS}}} \frac{\partial}{\partial p} \left(\frac{\rho_{\mathrm{OS}}}{\mu_{\mathrm{o}} B_{\mathrm{o}}} \right) \delta p + \frac{1}{K_{\mathrm{ro}}} \frac{\partial K_{\mathrm{ro}}}{\partial s_{\mathrm{w}}} \delta s_{\mathrm{w}} \right. \\ & \left. \left. + \frac{\mu_{\mathrm{o}} B_{\mathrm{o}}}{\rho_{\mathrm{OS}}} \frac{\partial}{\partial p_{\mathrm{b}}} \left(\frac{\rho_{\mathrm{OS}}}{\mu_{\mathrm{o}} B_{\mathrm{o}}} \right) \delta p_{\mathrm{b}} \right] \right\}_l^{(n+1)} \delta_{k,m} \, \mathrm{d}\mathbf{x} = Q_{\mathrm{L},k}. \end{aligned}$$

A.2. Saturated state

Under the saturated state, the unknowns are $p = p_{\mathrm{o}}$, s_{w}, and s_{o}. In a similar manner as in Appendix A.1, the integral forms of the governing equations can be linearized. For the water component, the form is the same as that in the undersaturated state. For the oil component, we have

$$\begin{aligned} & \int_{\partial V_i} \left\{ \frac{K K_{\mathrm{ro}}}{\mu_{\mathrm{o}}} \frac{\rho_{\mathrm{OS}}}{B_{\mathrm{o}}} + K K_{\mathrm{ro}} \frac{\partial}{\partial p} \left(\frac{\rho_{\mathrm{OS}}}{\mu_{\mathrm{o}} B_{\mathrm{o}}} \right) \delta p - \frac{K \rho_{\mathrm{OS}}}{\mu_{\mathrm{o}} B_{\mathrm{o}}} \frac{\partial K_{\mathrm{ro}}}{\partial s_{\mathrm{g}}} \delta s_{\mathrm{o}} + \frac{K \rho_{\mathrm{OS}}}{\mu_{\mathrm{o}} B_{\mathrm{o}}} \left(\frac{\partial K_{\mathrm{ro}}}{\partial s_{\mathrm{w}}} - \frac{\partial K_{\mathrm{ro}}}{\partial s_{\mathrm{g}}} \right) \delta s_{\mathrm{w}} \right\}_l^{(n+1)} (\nabla \Phi_{\mathrm{o}})_l^{(n+1)} \cdot \mathbf{n} \, \mathrm{d}A \\ & + \int_{\partial V_i} [H_{\mathrm{o}}^2]_l^{(n+1)} \cdot \mathbf{n} \, \mathrm{d}A + \sum_{k=1}^{N_{\mathrm{w}}} \sum_{m=1}^{M_{\mathrm{w},k}} \int_{V_i} \left\{ q_{\mathrm{o},k,m} + \frac{\mu_{\mathrm{o}} B_{\mathrm{o}}}{\rho_{\mathrm{OS}}} q_{\mathrm{o},k,m} \frac{\partial}{\partial p} \left(\frac{\rho_{\mathrm{OS}}}{\mu_{\mathrm{o}} B_{\mathrm{o}}} \right) \delta p - \frac{q_{\mathrm{o},k,m}}{K_{\mathrm{ro}}} \frac{\partial K_{\mathrm{ro}}}{\partial s_{\mathrm{g}}} \delta s_{\mathrm{o}} \right. \\ & \left. + \frac{q_{\mathrm{o},k,m}}{K_{\mathrm{ro}}} \left(\frac{\partial K_{\mathrm{ro}}}{\partial s_{\mathrm{w}}} - \frac{\partial K_{\mathrm{ro}}}{\partial s_{\mathrm{g}}} \right) \delta s_{\mathrm{w}} + \mathrm{WI}_{k,m} \frac{K_{\mathrm{ro}} \rho_{\mathrm{OS}}}{\mu_{\mathrm{o}} B_{\mathrm{o}}} (\delta p_{\mathrm{bh},k} - \delta p) \right\}_l^{(n+1)} \delta_{k,m} \, \mathrm{d}\mathbf{x} \\ & = \frac{V_i}{\Delta t_n} \left\{ H_{o,l}^{4,n+1} + \left(\phi \frac{\rho_{\mathrm{OS}}}{B_{\mathrm{o}}} \right)_l^{(n+1)} (\delta s_{\mathrm{o}})_l^{(n+1)} \right\}_{\mathbf{x}=\mathbf{x}_i}, \end{aligned}$$

and, for the gas component,

$$
\begin{aligned}
&\int_{\partial V_i}\left\{\frac{KK_{\mathrm{rg}}}{\mu_{\mathrm{g}}}\frac{\rho_{\mathrm{GS}}}{B_{\mathrm{g}}}+KK_{\mathrm{rg}}\frac{\partial}{\partial p}\left(\frac{\rho_{\mathrm{GS}}}{\mu_{\mathrm{g}}B_{\mathrm{g}}}\right)\delta p-\frac{K\rho_{\mathrm{GS}}}{\mu_{\mathrm{g}}B_{\mathrm{g}}}\frac{\partial K_{\mathrm{rg}}}{\partial s_{\mathrm{g}}}\delta s_{\mathrm{w}}-\frac{K\rho_{\mathrm{GS}}}{\mu_{\mathrm{g}}B_{\mathrm{g}}}\frac{\partial K_{\mathrm{rg}}}{\partial s_{\mathrm{g}}}\delta s_{\mathrm{o}}\right\}_l^{(n+1)}(\nabla\Phi_{\mathrm{g}})_l^{(n+1)}\cdot\mathbf{n}\,\mathrm{d}A\\
&+\int_{\partial V_i}\left[\frac{KK_{\mathrm{rg}}}{\mu_{\mathrm{g}}}\frac{\rho_{\mathrm{GS}}}{B_{\mathrm{g}}}\nabla(\delta p)\right]_l^{(n+1)}\cdot\mathbf{n}\,\mathrm{d}A-\int_{\partial V_i}\left[\frac{KK_{\mathrm{rg}}}{\mu_{\mathrm{g}}}\frac{\rho_{\mathrm{GS}}}{B_{\mathrm{g}}}\nabla\left(\frac{\partial p_{\mathrm{cgo}}}{\partial s_{\mathrm{g}}}\delta s_{\mathrm{w}}+\frac{\partial p_{\mathrm{cgo}}}{\partial s_{\mathrm{g}}}\delta s_{\mathrm{o}}\right)\right]_l^{(n+1)}\cdot\mathbf{n}\,\mathrm{d}A\\
&+\int_{\partial V_i}\left\{\frac{KK_{\mathrm{ro}}}{\mu_{\mathrm{o}}}\frac{R_{\mathrm{so}}\rho_{\mathrm{GS}}}{B_{\mathrm{o}}}+KK_{\mathrm{ro}}\frac{\partial}{\partial p}\left(\frac{R_{\mathrm{so}}\rho_{\mathrm{GS}}}{\mu_{\mathrm{o}}B_{\mathrm{o}}}\right)\delta p-\frac{KR_{\mathrm{so}}\rho_{\mathrm{GS}}}{\mu_{\mathrm{o}}B_{\mathrm{o}}}\frac{\partial K_{\mathrm{ro}}}{\partial s_{\mathrm{g}}}\delta s_{\mathrm{o}}\right.\\
&\left.+\frac{KR_{\mathrm{so}}\rho_{\mathrm{GS}}}{\mu_{\mathrm{o}}B_{\mathrm{o}}}\left(\frac{\partial K_{\mathrm{ro}}}{\partial s_{\mathrm{w}}}-\frac{\partial K_{\mathrm{ro}}}{\partial s_{\mathrm{g}}}\right)\delta s_{\mathrm{w}}\right\}_l^{(n+1)}(\nabla\Phi_{\mathrm{o}})_l^{(n+1)}\cdot\mathbf{n}\,\mathrm{d}A+\int_{\partial V_i}\left[\frac{KK_{\mathrm{ro}}}{\mu_{\mathrm{o}}}\frac{R_{\mathrm{so}}\rho_{\mathrm{GS}}}{B_{\mathrm{o}}}\nabla(\delta p)\right]_l^{(n+1)}\cdot\mathbf{n}\,\mathrm{d}A\\
&+\sum_{k=1}^{N_{\mathrm{w}}}\sum_{m=1}^{M_{\mathrm{w},k}}\int_{V_i}\left\{q_{\mathrm{g},k,m}^{\mathrm{G}}+\mathrm{WI}_{k,m}\frac{K_{\mathrm{rg}}\rho_{\mathrm{GS}}}{\mu_{\mathrm{g}}B_{\mathrm{g}}}(\delta p_{\mathrm{bh},k}-\delta p)+\frac{\mu_{\mathrm{g}}B_{\mathrm{g}}}{\rho_{\mathrm{GS}}}q_{\mathrm{g},k,m}^{\mathrm{G}}\frac{\partial}{\partial p}\left(\frac{\rho_{\mathrm{GS}}}{\mu_{\mathrm{g}}B_{\mathrm{g}}}\right)\delta p\right.\\
&\left.-\frac{q_{\mathrm{g},k,m}^{\mathrm{G}}}{K_{\mathrm{rg}}}\frac{\partial K_{\mathrm{rg}}}{\partial s_{\mathrm{g}}}(\delta s_{\mathrm{w}}+\delta s_{\mathrm{o}})\right\}_l^{(n+1)}\delta_{k,m}\,\mathrm{d}\mathbf{x}+\sum_{k=1}^{N_{\mathrm{w}}}\sum_{m=1}^{M_{\mathrm{w},k}}\int_{V_i}\left\{q_{\mathrm{o},k,m}^{\mathrm{G}}+\mathrm{WI}_{k,m}\frac{K_{\mathrm{ro}}R_{\mathrm{so}}\rho_{\mathrm{GS}}}{\mu_{\mathrm{o}}B_{\mathrm{o}}}(\delta p_{\mathrm{bh},k}-\delta p)\right.\\
&\left.-\frac{q_{\mathrm{o},k,m}^{\mathrm{G}}}{K_{\mathrm{ro}}}\frac{\partial K_{\mathrm{ro}}}{\partial s_{\mathrm{g}}}\delta s_{\mathrm{o}}+\frac{\mu_{\mathrm{o}}B_{\mathrm{o}}}{R_{\mathrm{so}}\rho_{\mathrm{GS}}}q_{\mathrm{o},k,m}^{\mathrm{G}}\frac{\partial}{\partial p}\left(\frac{R_{\mathrm{so}}\rho_{\mathrm{GS}}}{\mu_{\mathrm{o}}B_{\mathrm{o}}}\right)\delta p+\frac{q_{\mathrm{o},k,m}^{\mathrm{G}}}{K_{\mathrm{ro}}}\left(\frac{\partial K_{\mathrm{ro}}}{\partial s_{\mathrm{w}}}-\frac{\partial K_{\mathrm{ro}}}{\partial s_{\mathrm{g}}}\right)\delta s_{\mathrm{w}}\right\}_l^{(n+1)}\delta_{k,m}\,\mathrm{d}\mathbf{x}\\
&=\frac{V_i}{\Delta t_n}\left\{\left(\phi\frac{\rho_{\mathrm{GS}}}{B_{\mathrm{g}}}s_{\mathrm{g}}\right)_l^{(n+1)}-\left(\phi\frac{\rho_{\mathrm{GS}}}{B_{\mathrm{g}}}s_{\mathrm{g}}\right)^{(n)}-\left(\phi\frac{\rho_{\mathrm{GS}}}{B_{\mathrm{g}}}\right)_l^{(n+1)}(\delta s_{\mathrm{w}})_l^{(n+1)}\right.\\
&\left.+\left[c_r\phi_a\frac{\rho_{\mathrm{GS}}}{B_{\mathrm{g}}}s_{\mathrm{g}}+\phi s_{\mathrm{g}}\frac{\partial}{\partial p}\left(\frac{\rho_{\mathrm{GS}}}{B_{\mathrm{g}}}\right)\right]_l^{(n+1)}(\delta p)_l^{(n+1)}-\left(\phi\frac{\rho_{\mathrm{GS}}}{B_{\mathrm{g}}}\right)_l^{(n+1)}(\delta s_{\mathrm{o}})_l^{(n+1)}\right\}_{\mathbf{x}=\mathbf{x}_i}\\
&+\frac{V_i}{\Delta t_n}\left\{\left(\phi\frac{R_{\mathrm{so}}\rho_{\mathrm{GS}}}{B_{\mathrm{o}}}s_{\mathrm{o}}\right)_l^{(n+1)}-\left(\phi\frac{R_{\mathrm{so}}\rho_{\mathrm{GS}}}{B_{\mathrm{o}}}s_{\mathrm{o}}\right)^{(n)}\right.\\
&\left.+\left[c_r\phi_a\frac{R_{\mathrm{so}}\rho_{\mathrm{GS}}}{B_{\mathrm{o}}}s_{\mathrm{o}}+\phi s_{\mathrm{o}}\frac{\partial}{\partial p}\left(\frac{R_{\mathrm{so}}\rho_{\mathrm{GS}}}{B_{\mathrm{o}}}\right)\right]_l^{(n+1)}(\delta p)_l^{(n+1)}+\left(\phi\frac{R_{\mathrm{so}}\rho_{\mathrm{GS}}}{B_{\mathrm{o}}}\right)_l^{(n+1)}(\delta s_{\mathrm{o}})_l^{(n+1)})_l^{(n+1)}\right\}_{\mathbf{x}=\mathbf{x}_i}.
\end{aligned}
$$

Under the saturated state, the bottom hole pressure and water injection rate controls have the same form as those under the undersaturated state. The gas injection and production rate controls are, respectively, treated as

$$
\begin{aligned}
&\sum_{m=1}^{M_{\mathrm{w},k}}\int_{V_{k,m}}\left\{\mathrm{WI}_{k,m}\frac{K_{\mathrm{rgmax}}\rho_{\mathrm{GS}}}{\mu_{\mathrm{g}}B_{\mathrm{g}}}(\delta p_{\mathrm{bh},k}-\delta p)+q_{g,k,m}^{\mathrm{G}}\left[1+\frac{\mu_{\mathrm{g}}B_{\mathrm{g}}}{\rho_{\mathrm{GS}}}\frac{\partial}{\partial p}\left(\frac{\rho_{\mathrm{GS}}}{\mu_{\mathrm{g}}B_{\mathrm{g}}}\right)\delta p\right.\right.\\
&\left.\left.-\frac{1}{K_{\mathrm{rg}}}\frac{\partial K_{\mathrm{rg}}}{\partial s_{\mathrm{g}}}(\delta s_{\mathrm{w}}+\delta s_{\mathrm{o}})\right]\right\}_l^{(n+1)}\delta_{k,m}\,\mathrm{d}\mathbf{x}=Q_{\mathrm{G},k},
\end{aligned}
$$

and

$$\sum_{m=1}^{M_{w,k}} \int_{V_{k,m}} \left\{ \mathrm{WI}_{k,m} \left[\frac{K_{rg}\rho_{GS}}{\mu_g B_g} + \frac{K_{ro}R_{so}\rho_{GS}}{\mu_o B_o} \right] (\delta p_{bh,k} - \delta p) + q^G_{g,k,m} \left[1 + \frac{\mu_g B_g}{\rho_{GS}} \frac{\partial}{\partial p} \left(\frac{\rho_{GS}}{\mu_g B_g} \right) \delta p \right.\right.$$
$$\left. - \frac{1}{K_{rg}} \frac{\partial K_{rg}}{\partial s_g} (\delta s_w + \delta s_o) \right] + q^G_{o,k,m} \left[1 + \frac{\mu_o B_o}{R_{so}\rho_{GS}} \frac{\partial}{\partial p} \left(\frac{R_{so}\rho_{GS}}{\mu_o B_o} \right) \delta p + \frac{1}{K_{ro}} \left(\frac{\partial K_{ro}}{\partial s_w} - \frac{\partial K_{ro}}{\partial s_g} \right) \delta s_w \right.$$
$$\left.\left. - \frac{1}{K_{ro}} \frac{\partial K_{ro}}{\partial s_g} \delta s_o \right] \right\}_l^{(n+1)} \delta_{k,m} \, \mathrm{d}\mathbf{x} = Q_{G,k}.$$

The oil and liquid production rate controls are, respectively, linearized by

$$\sum_{m=1}^{M_{w,k}} \int_{V_{k,m}} \left\{ \mathrm{WI}_{k,m} \frac{K_{ro}\rho_{OS}}{\mu_o B_o} (\delta p_{bh,k} - \delta p) + q_{o,k,m} \left[1 + \frac{\mu_o B_o}{\rho_{OS}} \frac{\partial}{\partial p} \left(\frac{\rho_{OS}}{\mu_o B_o} \right) \delta p \right.\right.$$
$$\left.\left. + \frac{1}{K_{ro}} \left(\frac{\partial K_{ro}}{\partial s_w} - \frac{\partial K_{ro}}{\partial s_g} \right) \delta s_w - \frac{1}{K_{ro}} \frac{\partial K_{ro}}{\partial s_g} \delta s_o \right] \right\}_l^{(n+1)} \delta_{k,m} \, \mathrm{d}\mathbf{x} = Q_{O,k},$$

and

$$\sum_{m=1}^{M_{w,k}} \int_{V_{k,m}} \left\{ \mathrm{WI}_{k,m} \left[\frac{K_{rw}\rho_{WS}}{\mu_w B_w} + \frac{K_{ro}\rho_{OS}}{\mu_o B_o} \right] (\delta p_{bh,k} - \delta p) + q_{wk,m} \left[1 + \frac{\mu_w B_w}{\rho_{WS}} \frac{\partial}{\partial p} \left(\frac{\rho_{WS}}{\mu_w B_w} \right) \delta p + \frac{1}{K_{rw}} \frac{\partial K_{rw}}{\partial s_w} \delta s_w \right] \right.$$
$$\left. + q_{ok,m} \left[1 + \frac{\mu_o B_o}{\rho_{OS}} \frac{\partial}{\partial p} \left(\frac{\rho_{OS}}{\mu_o B_o} \right) \delta p + \frac{1}{K_{ro}} \left(\frac{\partial K_{ro}}{\partial s_w} - \frac{\partial K_{ro}}{\partial s_g} \right) \delta s_w - \frac{1}{K_{ro}} \frac{\partial K_{ro}}{\partial s_g} \delta s_o \right] \right\}_l^{(n+1)} \delta_{k,m} \, \mathrm{d}\mathbf{x} = Q_{L,k}.$$

Appendix B. Discretization of the governing equations

As noted, the discretization method we use for the governing equations of the black-oil model is the CVFA method. We very briefly review the discretization of these equations by this method. For more details, refer to [16].

Let the lth iteration values of the water and oil potentials on boundary e_{ij} $(j = 1, 2, \ldots, N_i)$ of a control volume V_i at the $(n+1)$th time step be approximated by (2.17) and the lth iteration values of the increments δp, δs_w, and δp_b be approximated by (2.18), where N_i is the number of boundaries of V_i. Then the linearized governing equations under the undersaturated state given in Appendix A.1 can be discretized as follows:

$$\sum_{j=1}^{N_i} \sum_{r=0}^{R_{ij}} \int_{e_{ij}} \left\{ H^1_w \Phi^i_{w_{j,r}} + \frac{KK_{rw}}{\mu_w} \frac{\rho_{WS}}{B_w} (\delta p^i_{j,r}) \right\}_l^{(n+1)} \nabla \phi^i_{j,r}(\mathbf{x}) \cdot \mathbf{n} \, \mathrm{d}A$$
$$- \sum_{j=1}^{N_i} \sum_{r=0}^{R_{ij}} \int_{e_{ij}} \left[\frac{KK_{rw}}{\mu_w} \frac{\rho_{WS}}{B_w} \left(\frac{\partial p_{cow}}{\partial s_w} \delta s_w \right)^i_{j,r} \right]_l^{(n+1)} \nabla \phi^i_{j,r}(\mathbf{x}) \cdot \mathbf{n} \, \mathrm{d}A$$
$$+ \sum_{k=1}^{N_w} \sum_{m=1}^{M_{w,k}} \int_{V_i} \left\{ H^3_{w,k,m} \right\}_l^{(n+1)} \delta_{k,m} \, \mathrm{d}\mathbf{x} = \frac{V_i}{\Delta t_n} \left\{ H^{4,n+1}_{w,l} + \left(\phi \frac{\rho_{WS}}{B_w} \right)_l^{(n+1)} (\delta s_w)^{(n+1)}_l \right\}_{\mathbf{x}=\mathbf{x}_i},$$

$$\sum_{j=1}^{N_i}\sum_{r=0}^{R_{ij}}\int_{e_{ij}}\left\{\left(H_{\mathrm{o}}^{1}+KK_{\mathrm{ro}}\frac{\partial}{\partial p_{\mathrm{b}}}\left(\frac{\rho_{\mathrm{OS}}}{\mu_{\mathrm{o}}B_{\mathrm{o}}}\right)\delta p_{\mathrm{b}}\right)\Phi^{i}_{\mathrm{o}_{j,r}}+\frac{KK_{\mathrm{ro}}}{\mu_{\mathrm{o}}}\frac{\rho_{\mathrm{OS}}}{B_{\mathrm{o}}}(\delta p^{i}_{j,r})\right\}_{l}^{(n+1)}\nabla\phi^{i}_{j,r}(\mathbf{x})\cdot\mathbf{n}\,\mathrm{d}A$$
$$+\sum_{k=1}^{N_{\mathrm{w}}}\sum_{m=1}^{M_{\mathrm{w},k}}\int_{V_i}\left\{H^{3}_{\mathrm{o},k,m}+\frac{\mu_{\mathrm{o}}B_{\mathrm{o}}}{\rho_{\mathrm{OS}}}q_{\mathrm{o},k,m}\frac{\partial}{\partial p_{\mathrm{b}}}\left(\frac{\rho_{\mathrm{OS}}}{\mu_{\mathrm{o}}B_{\mathrm{o}}}\right)\delta p_{\mathrm{b}}\right\}_{l}^{(n+1)}\delta_{k,m}\,\mathrm{d}\mathbf{x}$$
$$=\frac{V_i}{\Delta t_n}\left\{H^{4,n+1}_{o,l}+\left[\phi s_{\mathrm{o}}\frac{\partial}{\partial p_{\mathrm{b}}}\left(\frac{\rho_{\mathrm{OS}}}{B_{\mathrm{o}}}\right)\right]_{l}^{(n+1)}(\delta p_{\mathrm{b}})_{l}^{(n+1)}-\left(\phi\frac{\rho_{\mathrm{OS}}}{B_{\mathrm{o}}}\right)_{l}^{(n+1)}(\delta s_{\mathrm{w}})_{l}^{(n+1)}\right\}_{\mathbf{x}=\mathbf{x}_i},$$

and

$$\sum_{j=1}^{N_i}\sum_{r=0}^{R_{ij}}\int_{e_{ij}}\left\{\frac{KK_{\mathrm{ro}}}{\mu_{\mathrm{o}}}\frac{R_{\mathrm{so}}\rho_{\mathrm{GS}}}{B_{\mathrm{o}}}+KK_{\mathrm{ro}}\frac{\partial}{\partial p}\left(\frac{R_{\mathrm{so}}\rho_{\mathrm{GS}}}{\mu_{\mathrm{o}}B_{\mathrm{o}}}\right)\delta p+\frac{KR_{\mathrm{so}}\rho_{\mathrm{GS}}}{\mu_{\mathrm{o}}B_{\mathrm{o}}}\frac{\partial K_{\mathrm{ro}}}{\partial s_{\mathrm{w}}}\delta s_{\mathrm{w}}\right.$$
$$\left.+KK_{\mathrm{ro}}\frac{\partial}{\partial p_{\mathrm{b}}}\left(\frac{R_{\mathrm{so}}\rho_{\mathrm{GS}}}{\mu_{\mathrm{o}}B_{\mathrm{o}}}\right)\delta p_{\mathrm{b}}\right\}_{l}^{(n+1)}(\Phi^{i}_{\mathrm{o}_{j,r}})_{l}^{(n+1)}\nabla\phi^{i}_{j,r}(\mathbf{x})\cdot\mathbf{n}\,\mathrm{d}A$$
$$+\sum_{j=1}^{N_i}\sum_{r=0}^{R_{ij}}\int_{e_{ij}}\left[\frac{KK_{\mathrm{ro}}}{\mu_{\mathrm{o}}}\frac{R_{\mathrm{so}}\rho_{\mathrm{GS}}}{B_{\mathrm{o}}}(\delta p^{i}_{j,r})\right]_{l}^{(n+1)}\nabla\phi^{i}_{j,r}(\mathbf{x})\cdot\mathbf{n}\,\mathrm{d}A$$
$$+\sum_{k=1}^{N_{\mathrm{w}}}\sum_{m=1}^{M_{\mathrm{w},k}}\int_{V_i}\left\{q^{\mathrm{G}}_{\mathrm{o},k,m}+\frac{\mu_{\mathrm{o}}B_{\mathrm{o}}}{R_{\mathrm{so}}\rho_{\mathrm{GS}}}q^{\mathrm{G}}_{\mathrm{o},k,m}\frac{\partial}{\partial p}\left(\frac{R_{\mathrm{so}}\rho_{\mathrm{GS}}}{\mu_{\mathrm{o}}B_{\mathrm{o}}}\right)\delta p+\frac{q^{\mathrm{G}}_{\mathrm{o},k,m}}{K_{\mathrm{ro}}}\frac{\partial K_{\mathrm{ro}}}{\partial s_{\mathrm{w}}}\delta s_{\mathrm{w}}\right.$$
$$\left.+\frac{\mu_{\mathrm{o}}B_{\mathrm{o}}}{R_{\mathrm{so}}\rho_{\mathrm{GS}}}q^{\mathrm{G}}_{\mathrm{o},k,m}\frac{\partial}{\partial p_{\mathrm{b}}}\left(\frac{R_{\mathrm{so}}\rho_{\mathrm{GS}}}{\mu_{\mathrm{o}}B_{\mathrm{o}}}\right)\delta p_{\mathrm{b}}+\mathrm{WI}_{k,m}\frac{K_{\mathrm{ro}}R_{\mathrm{so}}\rho_{\mathrm{GS}}}{\mu_{\mathrm{o}}B_{\mathrm{o}}}(\delta p_{\mathrm{bh},k}-\delta p)\right\}_{l}^{(n+1)}\delta_{k,m}\,\mathrm{d}\mathbf{x}$$
$$=\frac{V_i}{\Delta t_n}\left\{\left(\phi\frac{R_{\mathrm{so}}\rho_{\mathrm{GS}}}{B_{\mathrm{o}}}s_{\mathrm{o}}\right)_{l}^{(n+1)}-\left(\phi\frac{R_{\mathrm{so}}\rho_{\mathrm{GS}}}{B_{\mathrm{o}}}s_{\mathrm{o}}\right)^{(n)}+\left[c_r\phi_a\frac{R_{\mathrm{so}}\rho_{\mathrm{GS}}}{B_{\mathrm{o}}}s_{\mathrm{o}}+\phi s_{\mathrm{o}}\frac{\partial}{\partial p}\left(\frac{R_{\mathrm{so}}\rho_{\mathrm{GS}}}{B_{\mathrm{o}}}\right)\right]_{l}^{(n+1)}(\delta p)_{l}^{(n+1)}\right.$$
$$\left.-\left(\phi\frac{R_{\mathrm{so}}\rho_{\mathrm{GS}}}{B_{\mathrm{o}}}\right)_{l}^{(n+1)}(\delta s_{\mathrm{w}})_{l}^{(n+1)}+\left[\phi s_{\mathrm{o}}\frac{\partial}{\partial p_{\mathrm{b}}}\left(\frac{R_{\mathrm{so}}\rho_{\mathrm{GS}}}{B_{\mathrm{o}}}\right)\right]_{l}^{(n+1)}(\delta p_{\mathrm{b}})_{l}^{(n+1)}\right\}_{\mathbf{x}=\mathbf{x}_i}.$$

Similarly, using (2.20) and (2.21), the linearized governing equations under the saturated state given in Appendix A.2 can be discretized.

Appendix C. Pressure equations

We now derive the pressure equations in the sequential solution method.

For a fixed control volume V_i, $(\delta s^{i}_{\mathrm{w}_{j,r}})_{l}^{(n+1)}$ and $(\delta p^{i}_{\mathrm{b}_{j,r}})_{l}^{(n+1)}$ are set to zero in the left-hand sides of the linearized and discretized governing equations in the undersaturated state to obtain

$$\sum_{j=1}^{N_i}\sum_{r=0}^{R_{ij}}\int_{e_{ij}}\left\{\frac{KK_{\mathrm{rw}}}{\mu_{\mathrm{w}}}\frac{\rho_{\mathrm{WS}}}{B_{\mathrm{w}}}+KK_{\mathrm{rw}}\frac{\partial}{\partial p}\left(\frac{\rho_{\mathrm{WS}}}{\mu_{\mathrm{w}}B_{\mathrm{w}}}\right)\delta p\right\}_{l}^{(n+1)}(\Phi^{i}_{\mathrm{w}_{j,r}})_{l}^{(n+1)}\nabla\phi^{i}_{j,r}(\mathbf{x})\cdot\mathbf{n}\,\mathrm{d}A$$
$$+\sum_{j=1}^{N_i}\sum_{r=0}^{R_{ij}}\int_{e_{ij}}\left[\frac{KK_{\mathrm{rw}}}{\mu_{\mathrm{w}}}\frac{\rho_{\mathrm{WS}}}{B_{\mathrm{w}}}(\delta p^{i}_{j,r})\right]_{l}^{(n+1)}\nabla\phi^{i}_{j,r}(\mathbf{x})\cdot\mathbf{n}\,\mathrm{d}A+\sum_{k=1}^{N_{\mathrm{w}}}\sum_{m=1}^{M_{\mathrm{w},k}}\int_{V_i}\left\{q_{\mathrm{w},k,m}+\frac{\mu_{\mathrm{w}}B_{\mathrm{w}}}{\rho_{\mathrm{WS}}}q_{\mathrm{w},k,m}\frac{\partial}{\partial p}\left(\frac{\rho_{\mathrm{WS}}}{\mu_{\mathrm{w}}B_{\mathrm{w}}}\right)\delta p\right.$$
$$\left.+\mathrm{WI}_{k,m}\frac{K_{\mathrm{rw}}\rho_{\mathrm{WS}}}{\mu_{\mathrm{w}}B_{\mathrm{w}}}(\delta p_{\mathrm{bh},k}-\delta p)\right\}_{l}^{(n+1)}\delta_{k,m}\,\mathrm{d}\mathbf{x}=\frac{V_i}{\Delta t_n}\left\{H^{4,n+1}_{\mathrm{w},l}+\left(\phi\frac{\rho_{\mathrm{WS}}}{B_{\mathrm{w}}}\right)_{l}^{(n+1)}(\delta s_{\mathrm{w}})_{l}^{(n+1)}\right\}_{\mathbf{x}=\mathbf{x}_i},$$

$$\sum_{j=1}^{N_i}\sum_{r=0}^{R_{ij}}\int_{e_{ij}}\left\{\frac{KK_{\mathrm{ro}}}{\mu_{\mathrm{o}}}\frac{\rho_{\mathrm{OS}}}{B_{\mathrm{o}}}+KK_{\mathrm{ro}}\frac{\partial}{\partial p}\left(\frac{\rho_{\mathrm{OS}}}{\mu_{\mathrm{o}}B_{\mathrm{o}}}\right)\delta p\right\}_l^{(n+1)}(\Phi^i_{\mathrm{o}_{j,r}})_l^{(n+1)}\nabla\phi^i_{j,r}(\mathbf{x})\cdot\mathbf{n}\,\mathrm{d}A$$

$$+\sum_{j=1}^{N_i}\sum_{r=0}^{R_{ij}}\int_{e_{ij}}\left[\frac{KK_{\mathrm{ro}}}{\mu_{\mathrm{o}}}\frac{\rho_{\mathrm{OS}}}{B_{\mathrm{o}}}(\delta p^i_{j,r})\right]_l^{(n+1)}\nabla\phi^i_{j,r}(\mathbf{x})\cdot\mathbf{n}\,\mathrm{d}A$$

$$+\sum_{k=1}^{N_{\mathrm{w}}}\sum_{m=1}^{M_{\mathrm{w},k}}\int_{V_i}\left\{q_{\mathrm{o},k,m}-\mathrm{WI}_{k,m}\frac{K_{\mathrm{ro}}\rho_{\mathrm{OS}}}{\mu_{\mathrm{o}}B_{\mathrm{o}}}(\delta p-\delta p_{\mathrm{bh},k})+\frac{\mu_{\mathrm{o}}B_{\mathrm{o}}}{\rho_{\mathrm{OS}}}q_{\mathrm{o},k,m}\frac{\partial}{\partial p}\left(\frac{\rho_{\mathrm{OS}}}{\mu_{\mathrm{o}}B_{\mathrm{o}}}\right)\delta p\right\}_l^{(n+1)}\delta_{k,m}\,\mathrm{d}\mathbf{x}$$

$$=\frac{V_i}{\Delta t_n}\left\{H^{4,n+1}_{o,l}+\left[\phi s_{\mathrm{o}}\frac{\partial}{\partial p_{\mathrm{b}}}\left(\frac{\rho_{\mathrm{OS}}}{B_{\mathrm{o}}}\right)\right]_l^{(n+1)}(\delta p_{\mathrm{b}})_l^{(n+1)}-\left(\phi\frac{\rho_{\mathrm{OS}}}{B_{\mathrm{o}}}\right)_l^{(n+1)}(\delta s_{\mathrm{w}})_l^{(n+1)}\right\}_{\mathbf{x}=\mathbf{x}_i},$$

and

$$\sum_{j=1}^{N_i}\sum_{r=0}^{R_{ij}}\int_{e_{ij}}\left\{\frac{KK_{\mathrm{ro}}}{\mu_{\mathrm{o}}}\frac{R_{\mathrm{so}}\rho_{\mathrm{GS}}}{B_{\mathrm{o}}}+KK_{\mathrm{ro}}\frac{\partial}{\partial p}\left(\frac{R_{\mathrm{so}}\rho_{\mathrm{GS}}}{\mu_{\mathrm{o}}B_{\mathrm{o}}}\right)\delta p\right\}_l^{(n+1)}(\Phi^i_{\mathrm{o}_{j,r}})_l^{(n+1)}\nabla\phi^i_{j,r}(\mathbf{x})\cdot\mathbf{n}\,\mathrm{d}A$$

$$+\sum_{j=1}^{N_i}\sum_{r=0}^{R_{ij}}\int_{e_{ij}}\left[\frac{KK_{\mathrm{ro}}}{\mu_{\mathrm{o}}}\frac{R_{\mathrm{so}}\rho_{\mathrm{GS}}}{B_{\mathrm{o}}}(\delta p^i_{j,r})\right]_l^{(n+1)}\nabla\phi^i_{j,r}(\mathbf{x})\cdot\mathbf{n}\,\mathrm{d}A$$

$$+\sum_{k=1}^{N_{\mathrm{w}}}\sum_{m=1}^{M_{\mathrm{w},k}}\int_{V_i}\left\{q^{\mathrm{G}}_{\mathrm{o},k,m}+\frac{\mu_{\mathrm{o}}B_{\mathrm{o}}}{R_{\mathrm{so}}\rho_{\mathrm{GS}}}q^{\mathrm{G}}_{\mathrm{o},k,m}\frac{\partial}{\partial p}\left(\frac{R_{\mathrm{so}}\rho_{\mathrm{GS}}}{\mu_{\mathrm{o}}B_{\mathrm{o}}}\right)\delta p+\mathrm{WI}_{k,m}\frac{K_{\mathrm{ro}}R_{\mathrm{so}}\rho_{\mathrm{GS}}}{\mu_{\mathrm{o}}B_{\mathrm{o}}}(\delta p_{\mathrm{bh},k}-\delta p)\right\}_l^{(n+1)}\delta_{k,m}\,\mathrm{d}\mathbf{x}$$

$$=\frac{V_i}{\Delta t_n}\left\{\left(\phi\frac{R_{\mathrm{so}}\rho_{\mathrm{GS}}}{B_{\mathrm{o}}}s_{\mathrm{o}}\right)_l^{(n+1)}-\left(\phi\frac{R_{\mathrm{so}}\rho_{\mathrm{GS}}}{B_{\mathrm{o}}}s_{\mathrm{o}}\right)^{(n)}+\left[c_r\phi_a\frac{R_{\mathrm{so}}\rho_{\mathrm{GS}}}{B_{\mathrm{o}}}s_{\mathrm{o}}+\phi s_{\mathrm{o}}\frac{\partial}{\partial p}\left(\frac{R_{\mathrm{so}}\rho_{\mathrm{GS}}}{B_{\mathrm{o}}}\right)\right]_l^{(n+1)}(\delta p)_l^{(n+1)}\right.$$

$$\left.-\left(\phi\frac{R_{\mathrm{so}}\rho_{\mathrm{GS}}}{B_{\mathrm{o}}}\right)_l^{(n+1)}(\delta s_{\mathrm{w}})_l^{(n+1)}+\left[\phi s_{\mathrm{o}}\frac{\partial}{\partial p_{\mathrm{b}}}\left(\frac{R_{\mathrm{so}}\rho_{\mathrm{GS}}}{B_{\mathrm{o}}}\right)\right]_l^{(n+1)}(\delta p_{\mathrm{b}})_l^{(n+1)}\right\}_{\mathbf{x}=\mathbf{x}_i}.$$

To eliminate the unknowns $(\delta s_{\mathrm{w}})_l^{(n+1)}$ and $(\delta p_{\mathrm{b}})_l^{(n+1)}$ in the right-hand sides of the above equations, let

$$D_{1,i}=-\left(\phi\frac{\rho_{\mathrm{OS}}}{B_{\mathrm{o}}}\right)_l^{(n+1)}\left[\phi s_{\mathrm{o}}\frac{\partial}{\partial p_{\mathrm{b}}}\left(\frac{R_{\mathrm{so}}\rho_{\mathrm{GS}}}{B_{\mathrm{o}}}\right)\right]_l^{(n+1)}+\left(\phi\frac{R_{\mathrm{so}}\rho_{\mathrm{GS}}}{B_{\mathrm{o}}}\right)_l^{(n+1)}\left[\phi s_{\mathrm{o}}\frac{\partial}{\partial p_{\mathrm{b}}}\left(\frac{\rho_{\mathrm{OS}}}{B_{\mathrm{o}}}\right)\right]_l^{(n+1)},$$

$$D_{2,i}=-\frac{1}{D_{1,i}}\left(\phi\frac{\rho_{\mathrm{WS}}}{B_{\mathrm{w}}}\right)_l^{(n+1)}\left[\phi s_{\mathrm{o}}\frac{\partial}{\partial p_{\mathrm{b}}}\left(\frac{R_{\mathrm{so}}\rho_{\mathrm{GS}}}{B_{\mathrm{o}}}\right)\right]_l^{(n+1)},$$

and

$$D_{3,i}=\frac{1}{D_{1,i}}\left(\phi\frac{\rho_{\mathrm{WS}}}{B_{\mathrm{w}}}\right)_l^{(n+1)}\left[\phi s_{\mathrm{o}}\frac{\partial}{\partial p_{\mathrm{b}}}\left(\frac{\rho_{\mathrm{OS}}}{B_{\mathrm{o}}}\right)\right]_l^{(n+1)}.$$

Then multiply the second and third equations in this appendix by $D_{2,i}$ and $D_{3,i}$, respectively, and combine the resulting equations with the first equation to obtain the pressure equation for V_i. Analogously, $(\delta s_{\mathrm{w}})_l^{(n+1)}$ and $(\delta s_{\mathrm{o}})_l^{(n+1)}$ are set to zero in the left-hand sides of the linearized and discretized equations under the saturated state to obtain the pressure equations.

References

[1] K. Aziz, Reservoir simulation grids: opportunities and problems, in: SPE 25233, the 12th SPE Symposium on Reservoir Simulation held in New Orleans, LA, USA, February 28–March 3, 1993.
[2] K. Aziz, A. Settari, Petroleum Reservoir Simulation, Applied Science Publishers, London, 1979.
[3] G. Booch, J. Rumbaugh, I. Jacobson, The Unified Modelling Language User Guid, Addison-Wesley, Boston, 1998.
[4] Z. Chen, Formulations and numerical methods for the black-oil model in porous media, SIAM J. Numer. Anal. 38 (2000) 489–514.
[5] Z. Chen, G. Huan, B. Li, An improved IMPES method for two-phase flow in porous media, Transp. Porous Media (in press).
[6] Z. Chen, G. Qin, R.E. Ewing, Analysis of a compositional model for fluid flow in porous media, SIAM J. Appl. Math. 60 (2000) 747–777.
[7] K.H. Coats, IMPES Stability: The Stable Setp, Paper SPE 69225, presented at the SPE Reservoir Simulation Symposium held in Houston, TX, February 11–14, 2001.
[8] J. Douglas Jr., D.W. Peaceman, H.H. Rachford Jr., A method for calculating multi-dimensional immiscible displacement, Trans. SPE AIME 216 (1959) 297–306.
[9] P.A. Forsyth, A control volume finite element method for local mesh refinement, in: SPE 18415, the SPE Symposium on Reservoir Simulation in Houston, TX, February 6–8, 1989.
[10] L.S. Fung, A.D. Hiebert, L. Nghiem, Reservoir simulation with a control volume finite element method, in: SPE 21224, the 11th SPE Symposium on Reservoir Simulation, Anaheim, February 17–20, 1991.
[11] B. Heinrichs, Finite Difference Methods on Irregular Networks, Birkhauser, Basel, Boston, Stuttgart, 1987.
[12] G. Huan, Z. Chen, B. Li, Applications of the control volume function approximation method to reservoir simulations, in: Z. Chen, R.E. Ewing (Eds.), Fluid Flows and Transport in Porous Media, Mathematical and Numerical Treatment, Contemporary Mathematics, vol. 295, AMS, 2002, pp. 279–292.
[13] J.E. Killough, Ninth SPE comparative solution project: a reexamination of black-oil simulation, in: Paper SPE 29110, the 13th SPE Symposium on Reservoir Simulation held in San Antonio, TX, February 12–15, 1995.
[14] B. Li, Z. Chen, G. Huan, Control volume function approximation methods and their applications to modeling porous media flow I: The two-phase flow, Adv. Water Resour. 26 (2003) 435–444.
[15] B. Li, Z. Chen, G. Huan, Control volume function approximation methods and their applications to modeling porous media flow II: the black oil model, Adv. Water Resour. (submitted).
[16] R.C. MacDonald, K.H. Coats, Methods for numerical simulation of water and gas coning, Trans. SPE AIME 249 (1970) 425–436.
[17] D.W. Peaceman, Interpretation of well-block pressures in numerical reservoir simulation, in: SPE 6893, 52nd Annual Fall Technical Conference and Exhibition, Denver, 1977.
[18] T.F. Russell, Stability analysis and switching criteria for an adaptive implicit method based on the CFL condition, in: Paper SPE 18416, the SPE Symposium on Reservoir Simulation in Houston, TX, February 6–8, 1989.
[19] J.W. Sheldon, B. Zondek, W.T. Cardwell, One-dimensional, incompressible, non-capillary, two-phase fluid flow in a porous medium, Trans. SPE AIME 216 (1959) 290–296.
[20] J.A. Trangenstein, J.B. Bell, Mathematical structure of the black-oil model for petroleum reservoir simulation, SIAM J. Appl. Math. 49 (1989) 749–783.
[21] J.A. Trangenstein, J.B. Bell, Mathematical structure of compositional reservoir simulation, SIAM J. Sci. Stat. Comput. 10 (1989) 817–845.
[22] S. Verma, K.A. Aziz, Control volume scheme for flexible grids in reservoir simulation, in: Paper SPE 37999, the 1997 SPE Symposium on Reservoir Simulation, Dallas, June 8–11, 1997.
[23] P.W. Vinsome, ORTHOMIN, An iterative method for solving sparse sets of simultaneous linear equations, in: Paper SPE 5729, presented at the SPE Symposium on Reservoir Simulation held in Los Angels, CA, February 19–20, 1976.
[24] L.C. Young, T.F. Russell, Implementation of an adaptive implicit method, in: Paper SPE 25245, the 12th SPE Symposium on Reservoir Simulation held in New Orleans, LA, February 28–March 3, 1993.